Tumour Suppressor Parafibromin/Hyrax Governs Cell Polarity and Centrosome Assembly in Neural Stem Cells

Qiannan Deng[1#], Cheng Wang[1#], Chwee Tat Koe[1,£], Jan Peter Heinen[2], Ye Sing Tan[1], Song Li[1], Cayetano Gonzalez[2,3], Wing-Kin Sung[4,5], and Hongyan Wang[1,6,7*]

[1] Neuroscience & Behavioral Disorders Programme, Duke-NUS Medical School, 8 College Road, Singapore 169857
[2] Institute for Research in Biomedicine, The Barcelona Institute of Science and Technology, Baldiri Reixac 10, 08028 Barcelona, Spain.
[3] Institució Catalana de Recerca i Estudis Avançats, ICREA, Passeig Lluıs Companys 23, 08010 Barcelona, Spain.
[£] Present address: [4]Genome Institute of Singapore, 60 Biopolis Street, Genome, Singapore 138672
[5] Department of Computer Science, National University of Singapore, Singapore
[6] Dept. of Physiology, Yong Loo Lin School of Medicine, National University of Singapore, Singapore 117597
[7] NUS Graduate School - Integrative Sciences and Engineering Programme (ISEP), National University of Singapore, Singapore 119077
[#] Equal contribution

* Lead contact: Hongyan Wang
* Correspondence: hongyan.wang@duke-nus.edu.sg

Running title
Hyx governs NSC polarity and centrosome assembly

SUMMARY

Neural stem cells (NSCs) divide asymmetrically to balance their self-renewal and differentiation. The imbalance can lead to NSC overgrowth and tumour formation. The function of Parafibromin, a conserved tumour suppressor, in the nervous system is not established. Here, we demonstrate that *Drosophila* Parafibromin/Hyrax (Hyx) inhibits NSC overgrowth by governing the cell polarity. Hyx is essential for the apicobasal polarity by localizing both apical and basal proteins asymmetrically in NSCs. *hyx* loss results in the symmetric division of NSCs, leading to the formation of supernumerary NSCs in the larval brain. Human Parafibromin fully rescues NSC overgrowth and cell polarity defects in *Drosophila hyx* mutant brains. Hyx plays a novel role in maintaining interphase microtubule-organizing center and mitotic spindle formation in NSCs. Hyx is required for the proper localization of a key centrosomal protein Polo and microtubule-binding proteins Msps and D-TACC in dividing NSCs. This study discovers that Hyx has a brain tumour suppressor-like function and maintains NSC polarity by regulating centrosome function and microtubule growth. The new paradigm that Parafibromin orchestrates cell polarity and centrosomal assembly may be relevant to Parafibromin/HRPT2-associated cancers.

Key Words

Drosophila, neural stem cells, neuroblasts, asymmetric division, microtubule growth, centrosome assembly

INTRODUCTION

Asymmetric division of neural stem cells (NSCs) is a fundamental strategy to balance self-renewal and differentiation during brain development. *Drosophila* neural stem cells (NSCs), also known as neuroblasts, have emerged as an excellent model for the study of stem cell self-renewal and tumourigenesis (Doe 2008, Januschke and Gonzalez 2008, Wu, Egger et al. 2008, Neumüller and Knoblich 2009, Chang, Wang et al. 2012). Each NSC divides asymmetrically to generate a self-renewing NSC and a neural progenitor that produces neurons/glia (Doe 2008). During asymmetric division, cell polarity is established by apically localized Par complex, including atypical PKC (aPKC), Bazooka (the *Drosophila* homologue of Par3), and Par6 (Wodarz, Ramrath et al. 1999, Wodarz, Ramrath et al. 2000, Petronczki and Knoblich 2001), as well as the Rho GTPase Cdc42 (Atwood, Chabu et al. 2007). This protein complex displaces the cell fate determinants Prospero, Numb and their adaptor proteins Miranda (Mira) and Partner of Numb to the basal cortex (Ikeshima-Kataoka, Skeath et al. 1997, Shen, Jan et al. 1997, Lu, Rothenberg et al. 1998, Matsuzaki, Ohshiro et al. 1998, Hannaford, Ramat et al. 2018). Linked to the Par proteins by Inscuteable (Insc), the protein complex of Pins, heterotrimeric G protein subunit Gαi and their regulators are recruited to the apical cortex during mitosis (Kraut, Chia et al. 1996, Schober, Schaefer et al. 1999, Yu, Morin et al. 2000, Schaefer, Petronczki et al. 2001, Yu, Wang et al. 2005, Bowman, Neumüller et al. 2006, Izumi, Ohta et al. 2006). Upon division, apical proteins are segregated exclusively into the larger NSC daughter to sustain self-renewal, and basal proteins into the smaller daughter cell to promote neuronal differentiation (Knoblich 2010, Chang, Wang et al. 2012). The mitotic spindle is oriented along the apicobasal axis to facilitate the asymmetric protein segregation (Berdnik and Knoblich 2002, Lee, Andersen et al. 2006, Gonzalez 2007, Wang, Ouyang et al. 2007, Doe 2008, Chabu and Doe 2009, Wang, Chang et al. 2009, Wang, Li et al. 2011). Failure of asymmetric division may result in cell fate transformation, leading to the formation of ectopic NSCs or the development of brain tumours (Caussinus and Gonzalez 2005, Bello, Reichert et al. 2006, Betschinger, Mechtler et al. 2006, Choksi, Southall et al. 2006, Lee, Andersen et al. 2006, Lee, Robinson et al. 2006, Lee, Wilkinson et al. 2006, Wang, Somers et al. 2006, Wang, Ouyang et al. 2007, Wang, Li et al. 2011).

Dysregulation of a few cell cycle regulators, such as Aurora-A kinase (AurA), Polo kinase (Polo), and Serine/Threonine protein phosphatase 2A (PP2A) result in a disruption of NSC asymmetry and microtubule function, leading to NSC overgrowth and brain tumor formation (Koe and Wang , Terada, Uetake et al. 2003, Wang, Somers et al. 2006, Wang, Ouyang et al. 2007, Chabu and Doe 2009, Krahn, Egger-Adam et al. 2009, Ogawa, Ohta et al. 2009, Wang, Chang et al. 2009, Januschke and Gonzalez 2010, Kelsom and Lu 2012). Moreover, ADP ribosylation factor like-2 (Arl2), a major regulator of microtubule growth, localizes Mini spindles/XMAP215/ch-TOG and Transforming acidic coiled-coil containing (D-TACC) to the centrosomes to control microtubule growth and cell polarity of NSCs (Chen, Koe et al. 2016).

Human Parafibromin/Cell division cycle 73 (Cdc73)/hyperparathyroidism type 2 (HRPT2) is a tumour suppressor that is linked to parathyroid carcinomas, the hyperparathyroidism-jaw tumour syndrome, breast, gastric, colorectal, lung cancers,

as well as head and neck squamous cell carcinomas (Selvarajan, Sii et al. 2008, Zheng, Takahashi et al. 2008, Newey, Bowl et al. 2009, Zhang, Yang et al. 2015). Somatic parafibromin mutations are found in 67-100% of sporadic parathyroid carcinomas (Newey, Bowl et al. 2009). Parafibromin is part of a conserved polymerase-associated factor complex that primarily regulates transcriptional events and histone modification (Wei, Yu et al. 1999, Rea, Eisenhaber et al. 2000). *Drosophila* Parafibromin/Hyx is essential for embryonic and wing development and positively regulates Wnt/Wingless signaling pathway in wing imaginal discs via a direct interaction with β-catenin/Armadillo. Human Parafibromin, but not yeast Cdc73, rescues the defects of wing development and embryonic lethality of *hyx* alleles (Mosimann, Hausmann et al. 2006), suggesting that Parafibromin has metazoan-specific functions during development. Interestingly, Parafibromin is expressed in both mouse and human brains, including the cortex, basal ganglia, cerebellum, and brainstem (Porzionato, Macchi et al. 2006), suggesting that Parafibromin may play a role in the central nervous system (CNS). However, the function of Parafibromin in the nervous system is not established.

Here, we provided the first evidence that Parafibromin/Hyx functions as a brain-tumor suppressor-like protein by regulating cell polarity and centrosomal function in NSCs. In a genetic screen, we isolated two *hyx* strong loss-of-function alleles that displayed NSC overgrowth in the larval brain. We show that Hyx is essential for apicobasal polarity of NSCs by ensuring the asymmetric distribution of apical and basal proteins. Remarkably, Hyx maintains interphase microtubule asters and is required for centrosome assembly and microtubule growth in NSCs. Hyx is required for the localization of centromomal protein Polo, Msps, and D-TACC in NSCs. Taken together, Parafibromin/Hyx plays a novel role in suppressing NSC overgrowth via governing cell polarity and centrosome assembly.

RESULTS

Loss of *hyx* results in NSC overgrowth in the larval central brain

In a clonal screen on a collection of chromosome 3R mutants induced by ethyl methanesulfonate (EMS) (Ly, Tan et al. 2019), we identified two new *hyrax* (*hyx*) alleles, hyx^{HT622} and $hyx^{w12\text{-}46}$ with a NSC overgrowth phenotype in the *Drosophila* larval central brain (Figure 1A-B). *hyx*/*CG11990* encodes a highly conserved 531-amino acid protein homologous to mammalian Parafibromin/Cdc73. hyx^{HT622} allele contains a 74-bp deletion from nucleotide 728 (immediately after amino acid 242) to 801, resulting in a frameshift and, in turn, the generation of a stop codon at amino acid 248, likely producing a truncated Hyx protein. The other new *hyx* allele, $hyx^{w12\text{-}46}$, carries two point mutations at nucleotide 1331 (T to G) and 1456 (T to A), which causes amino acid substitutions from Leucine (L) to Arginine (R) at 444 and Cysteine (C) to Serine (S) at 486. As hyx^{HT622} and $hyx^{w12\text{-}46}$ homozygotes are embryonically lethal, we generated MARCM (mosaic analysis with a repressible cell marker) clones (Lee and Luo 1999). Hyx protein in the clones was detected using guinea pig anti-Hyx antibodies we

generated against the N-terminal 1-176 amino acids of Hyx. In wild-type control clones, Hyx was predominantly localized to the nucleus of NSCs and their progeny (Figure S1A). In contrast, Hyx was undetectable in 91.3% of clones from *hyx*^{HT622} and 40% from *hyx*$^{w12-46}$ and was dramatically reduced in the rest of the clones (Figure S1A). Therefore, *hyx*^{HT622} and *hyx*$^{w12-46}$ are two strong loss-of-function alleles.

In the *Drosophila* larval central brain, both type I and type II NSCs divide asymmetrically (Bello, Izergina et al. 2008, Boone and Doe 2008, Bowman, Rolland et al. 2008). Each type I NSC generates another NSC and a ganglion mother cell (GMC) that gives rise to two neurons, while each type II NSC produces a NSC and a transient amplifying cell also known as an intermediate neural progenitor (INP) which, in turn, divide asymmetrically for a few rounds to produce GMCs (Bello, Izergina et al. 2008, Boone and Doe 2008, Bowman, Rolland et al. 2008, Weng, Golden et al. 2010). In the wild-type control, only one NSC is maintained in each type I or type II MARCM clones (Figure 1B). However, ectopic NSCs were observed in 87% of type I clones and 75% of type II clones from *hyx*^{HT622} (Figure 1B). Similarly, supernumerary NSCs were also observed in *hyx*$^{w12-46}$ clones in both type I and type II NSC lineages (Figure 1B). In addition, knockdown of *hyx* by two independent RNAi lines under the control of a NSC driver *insc*-Gal4 led to the formation of multiple NSCs in both types of lineages (Figure 1C). Moreover, the NSC overgrowth phenotype in *hyx*^{HT622} and *hyx*$^{w12-46}$ mutants was fully rescued by overexpression of a wild-type *hyx* transgene (Figure S1B-C). Therefore, *hyx* prevents NSC overgrowth in both type I and type II lineages.

Remarkably, the ectopic NSC phenotype observed in *hyx*^{HT622} larval brains was also completely rescued by overexpression of Parafibromin/HRPT2, the human counterpart of Hyx (Figure S1D). Likewise, the NSC overgrowth phenotype observed in *hyx* knockdown was fully restored by the introduction of human Parafibromin/HRPT2 in both type I and type II NSC lineages (Figure S1E). Taken together, Parafibromin/Hyx appears to have a conserved function in suppressing NSC overgrowth.

The PAF1 complex consists of the core subunits Paf1 (Antimeros/atms in *Drosophila*), Parafibromin/Cdc73 (Hyrax in *Drosophila*), Leo1 (Another transcription unit/Atu in *Drosophila*), Cln three requiring 9 (Ctr9), and Rtf1 (Mueller and Jaehning 2002, Zhu, Mandal et al. 2005). We sought to analyze the function of other components of the PAF1 complex in the larval central brains. Surprisingly, although Ctr9 is required to terminate the proliferation of *Drosophila* embryonic NSCs (Bahrampour and Thor 2016), no ectopic NSCs were observed in *ctr9*^{12P023} type I and type II MARCM clones (Figure S1F). Similarly, knockdown of *ctr9, atms*, or *atu* under the control of *insc*-Gal4 did not generate supernumerary NSCs in either type I or type II lineages in larval central brains (n=5 for all). Interestingly, knocking down *rtf* resulted in weak type II NSC overgrowth phenotype without affecting type I NSC lineage development (*rtf1* RNAi/BDSC#34586: type II, 31.2%, n=64 and *rtf1* RNAi/BDSC#34850: type II, 7%, n=43). Therefore, Parafibromin/Hyx is a key component of Paf1 complex that prevents NSC overgrowth in the brain.

Hyx is essential for the asymmetric division of NSCs

The ectopic NSCs in the absence of Hyx function was not due to INP dedifferentiation, as no type II NSCs were generated in INP clones from both control and *hyx* RNAi/V103555 (Figure S2A). Next, we assessed whether *hyx* is required for the asymmetric division of NSCs. In wild-type control metaphase NSCs, apical proteins such as aPKC, Insc, Baz/Par3, Par6, and Pins were localized asymmetrically (Figure 2A-F). By contrast, aPKC in hyx^{HT622} and hyx^{w12-46} metaphase NSCs were completely delocalized from the apical cortex to the cytoplasm (Figure 2A-B). Similarly, other apical proteins including Insc, Baz, Par6, and Pins in hyx^{HT622} metaphase NSCs were no longer asymmetric, exhibiting weak or punctate signals in the cytoplasm (Figure 2C-F).

Next, we examined the localization of basal proteins in *hyx* mutant NSCs. Mira was asymmetrically localized in 100% of wild-type NSCs during metaphase but was severely disrupted in metaphase NSCs of hyx^{HT622} and hyx^{w12-46} clones (Figure 2A-B). Similarly, Numb and Brat lost their asymmetry and were observed in the cytoplasm in metaphase NSCs from hyx^{HT622} clones (Figure 2C, G).

Similarly, *hyx* knockdown by two independent RNAi lines disrupted NSC apicobasal polarity. aPKC, Par6, Baz, Insc, and Pins were delocalized from the apical cortex in all metaphase NSCs for both *hyx* RNAi lines (Figure S2B-G). In addition, in metaphase NSCs upon *hyx* knockdown, Mira localization at the basal cortex was disrupted (Figure S2B-C). Moreover, Numb and Brat were also delocalized from the basal cortex in metaphase NSCs upon *hyx* knockdown (Figure S2D, H). Taken together, our data indicate that Hyx orchestrates cell polarity of NSCs by regulating the proper localization of both apical and basal proteins.

Given that cell polarity is essential for the asymmetric division of NSCs, we sought to investigate whether *hyx* depletion could result in the symmetric division of NSCs. To this end, we took advantage of a well-established Jupiter-GFP (also known as G147-GFP) under its endogenous promoter (Morin, Daneman et al. 2001). In live whole-mount larval brains that expressed G147-GFP, control NSCs always divided asymmetrically to produce two daughter cells with distinct cell sizes (Figure 2H, movie S1). By contrast, all NSCs in *hyx* RNAi divided symmetrically to generate two daughter cells with similar cell size (Figure 2H, movie S2). These observations indicate that *hyx*-depleted NSCs divide symmetrically, leading to NSC overgrowth.

Hyx maintains interphase microtubule asters and the mitotic spindle

We noticed that *hyx*-depleted NSCs formed shorter mitotic spindles. The mean spindle length in control metaphase NSCs was 9.81 ± 0.94 μm, whereas in *hyx* RNAi (V103555) the spindle length was dramatically shortened to 6.84 ± 1.46 μm (Figure 3A-B). Consistent with this observation, spindle length in metaphase hyx^{HT622} and hyx^{w12-46} NSCs were much shorter than that in the control (Figure 3C-D).

These observations prompted us to examine whether Hyx is important for microtubule assembly in NSCs. We sought to determine whether Hyx regulates the formation of microtubule asters in interphase NSCs. A wild-type interphase NSC forms one major microtubule aster marked by α-tubulin (α-tub). The microtubule aster is assembled by the microtubule-organizing center (MTOC)/ centrosome of cycling NSCs labeled by a centriolar protein Asterless (Asl; Figure 3E). Strikingly, the vast majority of interphase NSCs in hyx^{HT622} and hyx^{w12-46} clones either failed to organize a microtubule aster or formed a weak microtubule aster (Figure 3E). Likewise, during interphase, 50% of NSCs failed to form microtubule asters and 40.9% of NSCs only assembled weak microtubule asters upon *hyx* knockdown (Figure S3A). Therefore, Hyx is important for the formation of interphase microtubule asters.

The shortened mitotic spindle and the defects in the assembly of microtubule aster upon *hyx* depletion suggested that Hyx might regulate microtubule growth in dividing NSCs. To this end, we performed a microtubule regrowth assay by a “cold” treatment of larval brains on ice that efficiently depolymerized microtubules in NSCs, followed by a recovery at 25°C to allow microtubule regrowth in a time-course. In both control and *hyx* RNAi interphase NSCs upon the treatment on ice (t=0), no astral microtubules were observed and only weak residual microtubules labelled by α-tub remained at the centrosome (Figure 4A). The centrosome in 76.3% of these *hyx* RNAi interphase NSCs was absent or much smaller in size, suggesting that the MTOC was compromised upon *hyx* depletion (Figure 4A). In control interphase NSCs after returning to 25°C for various time points, robust astral microtubules were observed around the centrosome (Figure 4A). By contrast, following the recovery, the vast majority of *hyx* RNAi interphase NSCs reassembled scarce microtubule bundles without detectable MTOCs, even after 120 seconds (Figure 4A).

Next, we examined the microtubule regrowth in mitotic NSCs. Upon treatment on ice (t=0), in all control and *hyx* RNAi metaphase NSCs, spindle microtubules were effectively depolymerized with residual microtubules marking the centrosomes/spindle poles (Figure 4B). Consistent with poor centrosome assembly during interphase, the centrosomes of 98.0% of *hyx* RNAi metaphase NSCs were deformed with irregular shapes (Figure 4B). In all control metaphase NSCs following the recovery at 25°C, intense spindle microtubules were reassembled around centrosomes and chromosome mass from 30s onwards; the mitotic spindle completely re-formed at 2 min’s recovery (Figure 4B). In contrast, the majority of *hyx* RNAi metaphase NSCs assembled scarce spindle microtubule mass following the recovery; after 2 min’s recovery, only 14.6% of metaphase NSCs formed mitotic spindles, which were still shorter and thinner than the control; MTOCs remained weak or absent in these *hyx*-depleted NSCs (Figure 4B). Taken together, Hyx plays a central role in the formation of interphase microtubule asters and the mitotic spindle by promoting microtubule growth in NSCs.

Hyx is required for centrosome assembly in dividing NSCs

Since we demonstrate that the Hyx promotes microtubule growth and interphase aster formation in NSCs, we wondered whether Hyx regulates the assembly of the centrosomes, the major MTOC in dividing cells. Each centrosome is composed of a pair of centrioles surrounded by pericentriolar material (PCM) proteins. Centriolar proteins Spindle assembly abnormal 4 (Sas-4), Anastral spindle 2 (Ana2), and Asl are essential for centriole biogenesis and assembly (Varmark, Llamazares et al. 2007, Dzhindzhev, Yu et al. 2010, Wang, Li et al. 2011, Novak, Wainman et al. 2016, Gartenmann, Vicente et al. 2020). In control interphase and metaphase NSCs, Sas-4 was always observed at the centrosomes overlapping with Asl (Figure S3B-C). The localization of Sas-4 and Asl seemed unaffected at the centrosomes in both interphase and metaphase NSCs upon *hyx* knockdown (Figure S3B-C).

Wild-type NSCs typically contained two Asl-positive centrioles (Figure S3D-E), as the centrioles are duplicated early in the cell cycle. Strikingly, multiple centrioles marked by Asl at the centrosomes were observed in 47.1% of hyx^{HT622} clones (Figure S3D-E), 10.0% of $hyx^{w12\text{-}46}$ clones (n=8) and 12.9% of *hyx* RNAi NSCs (Figure S3F). Consistent with these observations, multiple centrioles were detected in 52.0% of S2 cells upon dsRNA treatment against *hyx* (Figure S3G-H), which was significantly higher than that in control (Figure S3G-H; 25.1%). These data suggest that Hyx might also affect centriole duplication.

Major PCM proteins γ-tubulin (γ-tub) and centrosomin (CNN), a CDK5RAP2 homolog, are essential for microtubule nucleation and anchoring. γ-tub is a component of the γ-tubulin ring complex (γ-TURC), the major microtubule nucleator in dividing cells including NSCs (Moritz, Braunfeld et al. 1995, Sunkel, Gomes et al. 1995). In control interphase and metaphase NSCs, robust γ-tub was detected at the centrosomes, co-localizing with Asl (Figure 5A). By contrast, γ-tub was absent or significantly reduced at the centrosomes in 95.7% of hyx^{HT622} and 54.8% of $hyx^{w12\text{-}46}$ interphase NSCs (Figure 5A). The fluorescence intensity of γ-tub was dramatically decreased in these NSCs from hyx^{HT622} and $hyx^{w12\text{-}46}$ clones (Figure 5A, C). In addition, γ-tub was strongly diminished at the centrosomes in 93.1% of hyx^{HT622} and 70.8% of $hyx^{w12\text{-}46}$ metaphase NSCs (Figure 5B). The protein levels of γ-tub protein dropped to “0.17” fold in hyx^{HT622} and “0.53” fold in $hyx^{w12\text{-}46}$ NSCs, respectively (Figure 5B-C). Likewise, γ-tub was strongly reduced at the centrosomes in 90.5% of interphase and 81.3% of metaphase NSCs upon *hyx* RNAi knockdown (Figure S4A-B). Moreover, the fluorescence intensity of γ-tub was dramatically decreased at the centrosomes in *hyx* RNAi interphase and metaphase NSCs (Figure S4A-C).

Next, we examined the localization of CNN, another essential PCM component. During interphase, 98.0% of control interphase NSCs had intense CNN signal at the centrosomes marked by Asl (Figure S4D, F). By contrast, CNN was barely detectable at the centrosomes in 84.8% of hyx^{HT622} and 58.3% of $hyx^{w12\text{-}46}$ (n=12) interphase NSCs (Figure S4D, F). Likewise, the protein levels of CNN were significantly diminished at the centrosomes in 72.4% of hyx^{HT622} and 66.7% of $hyx^{w12\text{-}46}$ (n=18) metaphase NSCs (Figure S4E-F). Consistent with these observations, upon *hyx* knockdown, CNN

protein levels were dramatically reduced from the centrosomes in 92.6% of interphase NSCs (Figure S4G, I). In metaphase NSCs with *hyx* knockdown, CNN intensity was also significantly dropped at the centrosomes in 46.7% of NSCs, albeit with a slightly weaker effect (Figure S5H-I). Therefore, Hyx ensures the recruitment of PCM proteins γ-tub and CNN to the centrosomes in both interphase and mitotic NSCs.

Centrosomal localization of Msps, D-TACC, and Polo is dependent on Hyx function in NSCs

Mini spindles (Msps) is an XMAP215/ch-TOG family protein and a key microtubule polymerase that controls microtubule growth and asymmetric division of NSCs in *Drosophila* larval central brains (Lee, Gergely et al. 2001, Chen, Koe et al. 2016). In control interphase NSCs, Msps co-localized with Asl at the centrosomes (Figure 5D). However, during interphase, Msps was delocalized from the centrosomes in 86.4% of hyx^{HT622} and 42.9% of $hyx^{w12\text{-}46}$ NSCs (Figure 5D). Likewise, during metaphase, Msps was nearly absent at the centrosomes in 87.5% of hyx^{HT622} and 60.0% of $hyx^{w12\text{-}46}$ NSCs (Figure 5E). Moreover, Msps was undetectable at the centrosomes in the majority of interphase NSCs upon *hyx* knockdown (Figure S5A, C). In metaphase NSCs, Msps was detected at the centrosomes only in 16.4% of *hyx* RNAi NSCs (Figure S5B-C).

As the efficient centrosomal localization of Msps depends on D-TACC, a microtubule-binding centrosomal protein (Lee, Gergely et al. 2001), we wondered whether D-TACC localization in NSCs requires Hyx function. In all control interphase NSCs, D-TACC was concentrated at the centrosomes marked by Asl (Figure S5D). Remarkably, during interphase, D-TACC was absent from the centrosomes in 92.0% of hyx^{HT622} (Figure S5D) and 81.8% of $hyx^{W12\text{-}46}$ NSCs (n=22). Similarly, in metaphase NSCs, D-TACC was undetectable at the centrosomes in 95.2% of hyx^{HT622} NSCs (Figure S5E) and 80.0% of $hyx^{w12\text{-}46}$ NSCs (n=15). Likewise, D-TACC was apparently undetectable at the centrosomes in the majority of interphase and metaphase NSCs upon *hyx* knockdown (Figure S5G-H). The fluorescence intensity of DTACC was significantly decreased in *hyx*-depleted NSCs (Figure S5F-I). Taken together, Hyx is essential for centrosomal localization of Msps and D-TACC in cycling NSCs.

As Polo is critical for the assembly of interphase microtubule asters and the asymmetric division (Rusan and Peifer 2007, Wang, Ouyang et al. 2007), we tested whether Hyx regulates the localization of Polo at the centrosomes. In control interphase NSCs, Polo was usually strongly detected at the centrosome marked by Asl (Figure 6A). In contrast, Polo was almost completely absent in 86.8% of hyx^{HT622} and 58.8% of $hyx^{w12\text{-}46}$ interphase NSCs (Figure 6A). In metaphase NSCs, Polo mainly appeared on the centrosomes, kinetochores, and weakly on the mitotic spindle (Figure 6B). In contrast, 80.0% of hyx^{HT622} and 75% of $hyx^{w12\text{-}46}$ metaphase NSCs lost Polo loci, and the remaining metaphase NSCs only had weak Polo signal (Figure 6B). Similarly, upon *hyx* knockdown, Polo was almost completely lost in 84.6% of interphase NSCs

and 78.3% of metaphase NSCs at the centrosomes (Figure S6A-B). The fluorescence intensity of Polo was significantly reduced at the centrosomes in *hyx*-depleted interphase and metaphase NSCs (Figure 6C, S6C).

Centrosomal protein AurA inhibits NSC overgrowth and regulates the centrosome function by directing the centrosomal localization of DTACC and Msps (Giet, McLean et al. 2002, Wang, Somers et al. 2006). We sought to examine whether the centrosomal localization of AurA is dependent on Hyx. AurA is clearly observed at the centrosomes marked by Asl in control NSCs (Figure 6D). Remarkably, AurA was nearly undetectable at the centrosomes in 87.2% of hyx^{HT622} and 75.0% $hyx^{w12\text{-}46}$ interphase NSCs (Figure 6D). The fluorescence intensity of AurA was decreased to "0.11" fold" in hyx^{HT622} and "0.23" fold during $hyx^{w12\text{-}46}$ interphase NSCs, respectively (Figure 6D, F). Likewise, in metaphase, AurA protein levels were significantly reduced in 88.9% of hyx^{HT622} and 50% of $hyx^{w12\text{-}46}$ NSCs (Figure 6E-F). Likewise, AurA was diminished in 100% of interphase NSCs and 56.7% of metaphase upon *hyx* knockdown (Figure S6D-F). Taken together, Hyx is essential for centrosome assembly and function by recruiting major centrosomal proteins to the centrosomes in NSCs.

Hyx is required for centrosome assembly in S2 cells *in vitro*

To investigate whether Hyx plays a role in centrosome assembly in non-neuronal cells, we knocked down *hyx* in S2 cells by a dsRNA treatment. We found that a centriolar protein, Ana2, properly resided at the centrosomes in metaphase cells (Figure S6G). Therefore, Hyx is not essential for the localization of centriolar proteins, similar to our findings in NSCs. Next, we examined the localization of other centrosomal proteins in S2 cells. Remarkably, DTACC intensity was significantly decreased at the centrosomes upon *hyx* knockdown in metaphase S2 cells (Figure 7A-B). Consistent with these observations, the intensity of α-tub was decreased to "0.65" fold on mitotic spindle (Figure 7C-D). These *in vitro* data support our observations in the larval brain and indicate that Hyx regulates microtubule growth and localization of centrosomal proteins. Polo was not significantly reduced at the centrosomes of dividing cells from *hyx* knockdown cells (Figure 7A, E). Besides, γ-tub intensity at the centrosomes marked by Ana2 was similar to the control (Figure S6G-H). The different observations in S2 cells and larval brains are likely due to incomplete depletion of *hyx* in S2 cells and/or different underlying mechanisms *in vitro*.

To further probe how Hyx regulates the centrosome assembly, we examined the ultrastructure of CNN and γ-tub with the advantage of super-resolution imaging. In 97.9% and 97.5% of control metaphase cells, CNN and γ-tub formed "doughnut-like" ring shape surrounding centriolar protein Asl at the centrosomes (Figure 7F-G). Remarkably, in 50.4% of *hyx* knockdown cells, CNN and γ-tub failed to form a "doughnut"- or ring-like pattern in mitotic cells; rather, they formed irregular shape at the centrosomes (Figure 7F-G). These observations suggest that Hyx is required for the proper recruitment of CNN and γ-tub at the centrosomes in S2 cells.

DISCUSSION

In this study, we established the essential role of Hyrax (Hyx), the *Drosophila* ortholog of Parafibromin, during the development of the central nervous system. We show that Hyx functions as a brain tumour suppressor-like protein to govern NSC asymmetric division and to inhibit NSC overgrowth in *Drosophila* larval central brains. We also demonstrate that Hyx plays a novel function in the formation of interphase microtubule aster and mitotic spindle in NSCs. Particularly, Hyx is important for the localization of PCM proteins to the centrosomes in dividing NSCs and S2 cells. Therefore, this study, for the first time, demonstrates that Parafibromin/Hyx has a tumour suppressor-like function and plays a critical role in the asymmetric division, microtubule growth, and centrosomal assembly in NSCs.

Drosophila Hyx is essential for embryogenesis and wing development (Mosimann, Hausmann et al. 2006). We provide the first evidence that Hyx is crucial for *Drosophila* larval brain development. Hyx also plays a novel role in regulating NSC apicobasal polarity. We show that Hyx is essential for the localization of most apical and basal polarity proteins to the cortex of dividing NSCs. We also found that Hyx is required for the centrosomal localization of AurA and Polo kinases in NSCs, two brain tumor suppressor-like proteins that regulate asymmetric division of NSCs (Lee, Andersen et al. 2006, Wang, Ouyang et al. 2007). Therefore, our study also identifies a previously unknown link between Hyx and these cell cycle regulators, raising the interesting possibility that this link might apply to other types of dividing cells including cancer cells.

Human Parafibromin is a tumour suppressor in parathyroid carcinomas and many other types of cancers (Selvarajan, Sii et al. 2008, Zheng, Takahashi et al. 2008, Newey, Bowl et al. 2009, Zhang, Yang et al. 2015). Parafibromin primarily regulates transcriptional events and histone modification (Wei, Yu et al. 1999, Rea, Eisenhaber et al. 2000). Parafibromin also inhibits cell proliferation by the blockage of a G1 cyclin, Cyclin D1, and the c-myc proto-oncogene (Woodard, Lin et al. 2005, Lin, Zhang et al. 2008, Yang, Han et al. 2010). Our TaDa (Targeted DamID) analysis of Hyx did not yield any consistent binding sites in three different repeats (data not shown), implying that Hyx does not seem to bind to sequence-specific sites in NSCs. We could not perform Chromatin-immunoprecipitation (ChIP) experiments for Hyx, because anti-Hyx antibodies we generated did not work in IP. Whether Hyx controls centrosomal-related genes and NSC polarity genes in NSCs via its well-known function in the transcriptional regulation remains to be determined.

We provide compelling data that Hyx plays a novel role in regulating microtubule growth and centrosomal assembly in NSCs and S2 cells. Hyx is important for the formation of the interphase microtubule aster and the mitotic spindle. It is required for the centrosomal localization of major PCM proteins, including γ-tub and CNN, AurA, and Polo. AurA is known to recruit γ-TuRC (γ-tubulin ring complex), CNN, and DTACC to the centrosomes (Giet, McLean et al. 2002, Wang, Jiang et al. 2014). Therefore, Hyx might regulate the centrosomal recruitment of DTACC, Msps, γ-tub, and CNN

through AurA. Intriguingly, Hyx appears to prevent centriole overduplication, suggesting that Hyx may play a pleiotropic function in regulating the cell cycle. The new role of Hyx in regulating microtubule growth and asymmetric division of NSCs supports our previous finding that microtubules play an essential role in NSC polarity (Chen, Koe et al. 2016). In addition to its predominant localization and function in the nucleus, cytoplasmic Parafibromin regulates apoptosis by directly targeting p53 mRNA (Jo, Chung et al. 2014). Human Parafibromin directly interacts with actin-binding protein actinin-2 and actinin-3 during the differentiation of myoblasts (Agarwal, Simonds et al. 2008), suggesting that Parafibromin might regulate actin cytoskeleton. Interestingly, *C. elegans* Ctr9 is required for the microtubule organization in epithelial cells with unknown mechanisms during morphogenesis of the embryo without any obvious disruption on the actin cytoskeleton (Kubota, Tsuyama et al. 2014). Therefore, the function of Hyx/Parafibromin in regulating microtubule growth and centrosomal assembly is likely a general paradigm in cell division regulation, which might be dysregulated in cancer cells.

We demonstrate that Human Parafribromin can functionally substitute Hyx in *Drosophila* CNS. This is in line with a previous study that Human parafibromin but not yeast Cdc73 rescues the defects of wing development and embryonic lethality in *hyx* alleles (Mosimann, Hausmann et al. 2006). Parafibromin/HRPT-2 is expressed in both mouse and human brains (Porzionato, Macchi et al. 2006). Deletion of *Hrpt2* in mouse embryos results in early lethality and a developmental defect of the brain, suggesting that Parafibromin may play a role in CNS development (Wang, Bowl et al. 2008). Future investigation on the likely conserved function of mammalian Parafibormin in NSC divisions and microtubule growth is warranted.

ACKNOWLEDGMENTS

We thank Dr. Yu F. for providing the EMS mutant collection (on 3R chromosome) from which *hyx* alleles were isolated. We also thank the Bloomington Drosophila Stock Center, Vienna Drosophila Resource Center, Kyoto stock centre DGGR, and the Developmental Studies Hybridoma Bank for fly stocks and antibodies. This work is supported by Singapore Ministry of Education Tier 2 MOE2018-T2-2-047 to H.W. and Spanish Ministerio de Ciencia, Innovacion y Universidades (PGC2018-097372-B-100) to C.G.

AUTHOR CONTRIBUTIONS

Conceptualization, H.W., Q.D., and C.W.; Methodology, Data curation, and Formal analysis, Q.D., C.W., S.L., C.T., J.P.H., W-K.S., and Y.S.T.; Writing-Original draft, Q.D., C.W., and H.W.; Writing-Review & Editing, H.W., Q.D. and C.G.; Funding Acquisition, H.W. and C.G.; Resources, H.W.; Supervision, H.W.

DECLARATION OF INTERESTS

The authors declare no competing interests.

METHODS

Fly stocks and genetics

Fly stocks and genetic crosses were reared at 25°C unless otherwise stated. Fly stocks were kept in vials or bottles containing standard fly food (0.8% Drosophila agar, 5.8% Cornmeal, 5.1% Dextrose, and 2.4% Brewer's yeast). The following fly strains were used in this study: *insc*-Gal4 (BDSC#8751; 1407-Gal4), *insc*-Gal4, *UAS-Dicer2* with and without *UAS-CD8-GFP*, *Jupiter-GFP* (G147), UAS-*hyx*, *UAS-HRPT2* (Mosimann, Hausmann et al. 2006). The type II NSC driver: w; *UAS-Dicer 2*, *wor*-Gal4, *ase*-Gal80/CyO; *UAS-mCD8-GFP*/TM3, Ser (Neumüller, Richter et al. 2011).

The following stocks were obtained from Bloomington Drosophila Stock Center (BDSC): *UAS-Gal* RNAi (BDSC#50680; this stock is often used as a control UAS element to balance the total number of UAS elements), $ctr9^{12P023}$ (BDSC#59389), *rtf1* RNAi (BDSC#34586), *rtf1* RNAi (BDSC#34850), *rtf1* RNAi (BDSC#31718).

The following stocks were obtained from Vienna Drosophila Resource Center (VDRC): *hyx* RNAi (28318), *hyx* RNAi (103555), *atms* RNAi (108826), *atu* RNAi (17490), *atu* RNAi (106074), *ctr9* RNAi (108874), *ctr9* RNAi (Chaturvedi, Inaba et al. 2016), *rtf1* RNAi (27341), *rtf1* RNAi (110392).

All experiments were carried out at 25°C, except for RNAi knockdown or overexpression at 29°C.

Immunohistochemistry

Third-instar *Drosophila* larvae were dissected in PBS, and larval brains were fixed in 4% EM-grade formaldehyde in PBT (PBS + 0.3% Triton-100) for 22 min. The samples were processed for immunostaining as previously described (Li, Koe et al. 2017). For α-tubulin immunohistochemistry, larvae were dissected in Shield and Sang M3 medium (Sigma-Aldrich) supplemented with 10% FBS, followed by fixation in 10% formaldehyde in Testis buffer (183 mM KCl, 47 mM NaCl, 10 mM Tris-HCl, and 1 mM EDTA, pH 6.8) supplemented with 0.01% Triton X-100.) The fixed brains were washed once in PBS and twice in 0.1% Triton X-100 in PBS. Images were taken with an AxioCam HR camera, with 1.5× to 8× of digital zoom from an LSM710 confocal microscope system (Axio Observer Z1; ZEISS) using a Plan-Apochromat 40×/1.3 NA oil differential interference contrast objective, and brightness and contrast were adjusted by Adobe Photoshop or Fiji (imageJ).

The primary antibodies used were: rabbit affinity-purified anti-Hyx/Cdc73 (1: 1000; J. T. Lis); guinea pig anti-Dpn (1:1000), mouse anti-Mira (1:50; F. Matsuzaki), rabbit anti-Mira (1:500, W. Chia), anti-Insc (1:1000), rabbit anti-aPKCζ C20 (1:100; Santa Cruz Biotechnologies, Dallas, TX), guinea-pig anti-Numb (1:1000; J Skeath), rabbit anti-

GFP (1:3,000; F. Yu), mouse anti-GFP (1:5,000; F. Yu), rabbit anti-Asense (1:1000; YN Jan), guinea pig anti-Asl (1:200, C. Gonzalez), rabbit anti-Sas-4 (1:100, J. Raff), mouse anti-α-tubulin (1:200, Sigma, Cat#: T6199), mouse anti-γ-tubulin (1:200, Sigma, Cat#: T5326), rabbit anti-CNN (1:5000, E. Schejter and T. Megraw), rabbit anti-Msps (1:500), rabbit anti-Msps (1:1000, J. Raff), rabbit anti-PH3 (1:200, Sigma, Cat#: 06-570), rabbit anti-DTACC (1:200), rabbit anti-Ana2 (Wang, Li et al. 2011) (1:50), α-tubulin (1:200, Sigma, Cat#: T6199), rabbit anti-AurA (1:200, J. Raff), rat anti-CD8 (1:250, Caltag laboratories), mouse anti-Polo (1:30, C. Sunkel). The secondary antibodies used were conjugated with Alexa Fluor 488, 555, or 647 (Jackson laboratory).

Spinning-disc super-resolution imaging

Super-resolution Spinning disc confocal-structured illumination microscopy (SDC-SIM) was performed on a spinning disk system (Gataca Systems) based on an inverted microscope (Nikon Ti2-E; Nikon) equipped with a confocal spinning head (CSU-W; Yokogawa), a Plan-Apo objective (100x1.45-NA), a back-illuminated sCMOS camera (Prime95B; Teledyne Photometrics), and a super-resolution module (Live-SR; GATACA Systems) based on structured illumination with optical reassignment technique and online processing leading to a two-time resolution improvement (Roth and Heintzmann 2016). The maximum resolution is 128 nm with a pixel size in super-resolution mode of 64nm. Excitation light was provided by 488-nm/150mW (Vortran) (for GFP), 561-nm/100mW (Coherent) (for mCherry/mRFP/tagRFP) and 639-nm/150mW (Vortran) (for iRFP) laser combiner (iLAS system; GATACA Systems), and all image acquisition and processing were controlled by MetaMorph (Molecular Device) software. Images were further processed with imageJ.

Generation of guinea pig anti-Hyx antibodies

The cDNA region encoding the N-terminal 1-176 amino acid residues of Hyx/Cdc73 was amplified by PCR with the oligos: 5'TCCGAATTCATGGCAGATCCGCTCA GC3'and 5'ATGCGGCCGCCTACGTCTCGGACAGCGACTT3'. The PCR products were cloned into vector pMAL-c2x (Addgene # 75286). The fusion protein MBP-Hyx 1-176 was purified and injected into guinea pigs and purified by GenScript (Hong Kong).

Clonal analysis

MARCM clones were generated as previously described (Lee and Luo 1999). Briefly, larvae were heat-shocked at 37°C for 90 min at 24 hr ALH and 10–16 hr after the first heat shock. Larvae were further aged for 3 days at 25°C, and larval brains were dissected and processed for immunohistochemistry. To generate type II NSC clones, UAS lines were crossed to the type II driver at 25°C and shifted to 29°C at 24 hr ALH. Wandering third instar larvae were dissected after incubation for 3 or 4 days at 29°C.

Time-Lapse Recording

Time-lapse recording was performed as described (Chen, Koe et al. 2016). The whole-mount brain expressing G147-GFP was used to analyze the asymmetric cell division of NSCs. The brain was dissected and loaded into a Lab-TekTM chambered coverglass (Thermo Fisher Scientific) filled with dissecting medium supplemented with 2.5% methyl cellulose (Sigma-Aldrich). The time-lapse images of NSC division were acquired every

30 s on a confocal microscope (LSM 710; ZEISS). The video was processed with ImageJ and displayed at 15 frames per second.

Microtubule regrowth assay

Microtubule regrowth assay was performed as described previously (Chen, Koe et al. 2016). Third-instar larval brains were dissected in Shield and Sang M3 insect medium (Sigma-Aldrich) supplemented with 10% FBS, and microtubules were depolymerized by incubating the larval brains on ice for 40 min. The brains were allowed to recover at 25°C at various times to allow microtubule regrowth. The brains were immediately fixed in 10% formaldehyde in testis buffer (183 mM KCl, 47 mM NaCl, 10 mM Tris-HCl, and 1 mM EDTA, pH 6.8) supplemented with 0.01% Triton X-100. The fixed brains were washed once in PBS and twice in 0.1% Triton X-100 in PBS, followed by immunohistochemistry.

S2 cell culture, transfection, and quantitative RT-PCR

Cell culture. *Drosophila* S2 cells were cultured in Express Five SFM (Thermo Fisher Scientific) supplemented with 2 mM glutamine (Thermo Fisher Scientific) at 25°C.
dsRNA production. DNA fragments approximately 470 bp in length for dsEGFP as control and 825bp in length for dsHyx, were amplified by using PCR. Each primer used in the PCR contained a 5′ T7 RNA polymerase binding site (TAATACGACTCACTATAGGG) followed by sequences specific for the targeted genes. The PCR products were purified by using the QIAquick PCR Purification Kit (Cat No. 28106). The purified PCR products were used as templates by using a MEGASCRIPT T7 transcription kit (Ambion, Austin, TX) to produce dsRNA. The dsRNA products were ethanol-precipitated and resuspended in water. The dsRNAs were annealed by incubation at 65°C for 30 min followed by slow cooling to room temperature. one microgram of dsRNA was analyzed by 1% agarose gel electrophoresis to ensure that the majority of the dsRNA existed as a single band. The dsRNA was stored at −20°C. The primers used for dsRNA synthesis were ds-*egfp*-forward: 5' TCGTGACCACCCTGACCTAC -3'; ds-*egfp*-reverse: 5' - GCTTCTCGTTGGGGTCTTT- 3' and ds-*hyx*-forward: 5'- TGCTGCAACACTCGGTCTAC -3'; ds-*hyx*-reverse: 5' - GTGCTCCCGGTAGGTTGTTA- 3'.

Extraction of total messenger RNA (mRNA) and RT-PCR. Total mRNA from ds- *egfp* and ds-*hyx* treated S2 cells were extracted using TRI Reagent (Sigma-Aldrich) according to the manufacturer's instructions. Reverse transcription was performed with iScript™ cDNA Synthesis Kit (Bio-RAD) according to the manufacturer's instructions.

Quantification and statistical analysis

Drosophila larval brains from various genotypes were placed dorsal side up on confocal slides. The confocal z-stacks were taken from the surface to the deep layers of the larval brains. For each genotype, at least 10 NSCs were imaged and ImageJ or Zen software was used for quantifications.

Statistical analysis was essentially performed using GraphPad Prism 8. Unpaired two-tail t-tests were used for comparison of two sample groups, and one-way ANOVA or two-way ANOVA followed by Sidak's multiple comparisons test was used for comparison of more than two sample groups. All data are shown as the mean ± SD. Statistically nonsignificant (ns) denotes $P > 0.05$, * denotes $P < 0.05$, ** denotes $P < 0.01$, *** denotes $P < 0.001$, and **** denotes $P < 0.0001$. All experiments were performed with a minimum of two repeats. In general, n refers to the number of NSCs counted unless otherwise indicated.

Figure legends

Figure 1. Hyx regulates the homeostasis of central larval brain NSCs.

(A) An illustration of two *hyx* EMS alleles. (B) Type I and type II MARCM clones of various genotypes were labeled with Dpn, Ase, and CD8-GFP. Multiple NSCs were observed in *hyx*-depleted type I and type II MARCM clones. Type I clones: control (FRT82B), n=61; hyx^{HT622}, 87%, n=92; hyx^{w12-46}, 30.8%, n=68. Type II clones: control (FRT82B), n=57; hyx^{HT622}, 75%, n=75; 73.3%, hyx^{w12-46}, n=66. (C) Type I and type II NSC lineages of control (*UAS-β-Gal* RNAi), *hyx* RNAi (GD/V28318), and *hyx* RNAi (KK/V103555) under the control of *insc*-Gal4 driver were labeled with Dpn, Ase, and CD8-GFP. Ectopic NSCs were generated in *hyx* RNAi type I NSC lineages (control, 0%, n=57; GD, 43%, n=92; KK, 27%, n=73) and type II NSC lineages (control, 0%, n=64; GD, 72%, n=83; KK, 89.29%, n=56). MARCM clones in B and NSC lineages in C are outlined by dotted lines. Arrows in B, C indicate NSCs. Scale bars: 5μm.

Figure 2. Hyx is essential for asymmetric cell division of NSCs.

(A) Metaphase NSCs of control (FRT82B; n=50) and hyx^{HT622} MARCM clones were labeled with aPKC, Mira, and DNA. hyx^{HT622}, aPKC delocalization, 100%; Mira delocalization, 81.6%; n=49 for both. (B) Metaphase NSCs of control (FRT82B; n=45) and hyx^{W12-46} MARCM clones were labeled with aPKC, Mira, and DNA. 100% delocalization of aPKC and Mira in hyx^{W12-46}, n=50 for both. (C) Metaphase NSCs of control (FRT82B; n=47) and hyx^{HT622} MARCM clones were labeled with Insc, Numb, and DNA. 100% delocalization of Insc and Numb in hyx^{HT622}, n=49 for both. (D) Control (FRT82B; n=46) and hyx^{HT622} metaphase NSCs were labeled with Baz and DNA. 100% Baz delocalization in hyx^{HT622} (n=49). (E) Control (FRT82B; n=50) and hyx^{HT622} metaphase NSCs were labelled with Par6 and DNA. 100% delocalization of Par6 in hyx^{HT622} (n=49). (F) Metaphase NSCs from control (FRT82B) and hyx^{HT622} were labelled with Pins and DNA. 100% delocalization of Pins in hyx^{HT622}; n=49 for both genotypes. Clones were marked by CD8-GFP. (G) Metaphase NSCs from control (FRT82B; n=48) and hyx^{HT622} were labelled with Brat and DNA. 100% Brat delocalization in hyx^{HT622} (n=50). (H) Still images of time-lapse imaging of control (G147-GFP/+; n=15 and Video S1) and *hyx* RNAi (KK/V103555; n=5 and Video S2) NSCs expressing G147-GFP under the control of *insc*-Gal4 at 48h ALH. MARCM clones are marked by dotted lines (A, C-G). Scale bar: 5 μm.

Figure 3. Hyx is required for the formation of the microtubule aster and the mitotic spindle in NSCs.

(A) Metaphase NSCs of control (*UAS-β-Gal* RNAi; n=29) and *hyx* RNAi (KK/V103555; n=40) under the control of *insc*-Gal4 were labelled for α-tub and DNA. (B) Quantification of spindle length (with SD) in A. (C) NSCs of FRT82B control, hyx^{HT622},

and *hyx*$^{W12-46}$ MARCM clones were labelled for α-tub and DNA and CD8-GFP. (D) Quantification of spindle length (with SD) in C. Spindle length: control, 9.70± 1.13 μm, n=21; *hyx*^{HT622}, 6.13 ± 1.22 μm in n=18; *hyx*$^{W12-46}$, 7.43 ± 1.25 μm, n=18. (E) Interphase NSCs from control (FRT82B; n=11), *hyx*^{HT622} (n=24), and *hyx*$^{w12-46}$ (n=29) MARCM clones were labelled for α-tub, Asl, GFP, and PH3. NSCs failed to form a microtubule aster in 79.2% of *hyx*^{HT622} and 34.5% of *hyx*$^{w12-46}$ clones. The rest of them formed a weak microtubule aster. Cell outlines are indicated by the white dotted lines. Arrows indicate the centrosomes. Scale bars: 5 μm.

Figure 4. Hyx promotes microtubule growth in NSCs.

(A) Control (*UAS-β-Gal* RNAi) and *hyx* RNAi (KK/V103555) interphase NSCs were labelled for α-tub and DNA at various time points after recovery from treatment on ice in microtubule regrowth assay. At 0 second (t=0; ice treatment), no astral microtubules around the centrosome/MTOC were observed in all control (n=74) and *hyx* RNAi NSCs (n=63). At all subsequent time points following the recovery, all control NSCs assembled robust astral microtubules (t=30s, n=31; t=60s, n=11; t=90s, n=27; t=120s, n=26). Astral microtubules were lost in *hyx* RNAi: t=30 s, 71.9%, n=43; t=60 s, 85.7%, n=7; t=90 s, 91.2%, n=46; t=2 min, 86.3%, n=63. (B) Control (*UAS-β-Gal* RNAi) and *hyx* RNAi (KK/V103555) metaphase NSCs were labelled for α-tub and DNA at various time points after recovery from treatment on ice in microtubule regrowth assay. Control: t=0, n=52; t=30 s, n=19; t=60 s, n=9; t=90 s, n=41; *hyx* RNAi, t=0, n=28. Scarce spindle microtubule mass assembled in *hyx* RNAi: t=30 s, 91.7%, n=18; t=60 s, 66.7%, n=3; t=90 s, 69.7%, n=19; t=2 min, 85.4%, n=11. RNAi was controlled by *insc*-Gal4. Cell outlines are indicated by the white-dotted lines. Scale bars: 5 μm.

Figure 5. Hyx regulates the localization of centrosomal proteins γ-tubulin and Msps in NSCs.

(A) Interphase NSCs of MARCM clones in control (FRT82B) and *hyx*^{HT622} were labelled with γ-tub, Asl, GFP, and PH3. γ-tub delocalization: control, 3.8%, n=26; *hyx*^{HT622}, 95.7%, n=23; *hyx*$^{w12-46}$, 54.8%, n=42. (B) Metaphase NSCs of MARCM clones in control (FRT82B) and *hyx*^{HT622} were labelled for γ-tub, Asl, GFP, and PH3. γ-tub delocalization: control, 6.9%, n=29; *hyx*^{HT622}, 93.1%, n=29; *hyx*$^{w12-46}$, 70.8%, n=24. (C) Quantification graph of the fold change of γ-tub intensity in NSCs from A and B. (D) Interphase NSCs of MARCM clones in control (FRT82B) and *hyx*^{HT622} were analyzed by Msps, Asl, GFP, and PH3. Control, n=44; *hyx*^{HT622}, n=44; *hyx*$^{w12-46}$, n=7. (E) Metaphase NSCs of control (FRT82B; all NSCs have Msps localization at the centrosomes, n=32), *hyx*^{HT622} (n=24), and *hyx*$^{w12-46}$ (n=5) MARCM clones were labelled with Msps, Asl, GFP, and PH3. (F) Quantification graph of the fold change of Msps intensity in NSCs from D and E. Interphase: control, “1” fold, n=44; *hyx*^{HT622}: “0.14” fold, n=44; *hyx*$^{w12-46}$, “0.66” fold, n=7. Metaphase: control, “1” fold, n=32; *hyx*^{HT622}, “0.19” fold,

n=24; *hyx*$^{w12-46}$, “0.48” fold, n=5. Cell outlines are indicated by the white dotted lines. Arrows point at the centrosomes. Scale bars: 5 μm.

Figure 6. Hyx regulates the localization of centrosomal proteins Polo and AurA in NSCs.

(A) Interphase NSCs from control (FRT82B) and *hyx*^{HT622} MARCM clones were labelled with Polo, Asl, GFP, and PH3. Polo delocalization/reduction: control, 5.8%, n=52; *hyx*^{HT622}, n=38; *hyx*$^{w12-46}$, n=34. (B) Metaphase NSCs of FRT82B control, *hyx*^{HT622} and *hyx*$^{w12-46}$ MARCM clones were labelled with Polo, Asl, GFP and PH3. Polo delocalization/reduction: control, 0%, n=20; *hyx*^{HT622}, 80.0%, n=10; *hyx*$^{w12-46}$, 75.0%, n=12. (C) Quantification graph of the fold change of Polo intensity in NSCs from A and B. Interphase: control, “1” fold, n=41; *hyx*^{HT622}, “0.12” fold n=38; *hyx*$^{w12-46}$, “0.53” fold, n=34. Metaphase: control, “1” fold, n=20; *hyx*^{HT622}, “0.10” fold, n=10; *hyx*$^{w12-46}$, “0.46” fold, n=12. (D) Interphase NSCs from control (FRT82B; n=36) and *hyx*^{HT622} (n=39) MARCM clones were labelled with AurA, Asl, GFP, and PH3. (E) Metaphase NSCs of control (FRT82B; n=22) and *hyx*^{HT622} (n=18) MARCM clones were labelled with AurA, Asl, GFP, and PH3. (F) Quantification graph of the fold change of AurA intensity in NSCs from D and E. Interphase: control, “1” fold, n=36; *hyx*^{HT622}, “0.11” fold, n=39; *hyx*$^{w12-46}$, “0.23” fold, n=20. Metaphase: control, “1” fold, n=22; *hyx*^{HT622}, “0.43” fold, n=18; *hyx*$^{w12-46}$, “0.79” fold, n=8. Cell outlines are indicated by the white-dotted lines. Arrows point at centrosome in A. Scale bars: 5 μm.

Figure 7. Hyx is required for centrosome assembly in S2 cells *in vitro*.

(A) Metaphase cells from ds-*egfp*-treated S2 cells and ds-*hyx*-treated S2 cells were analyzed with DTACC, Polo, Asl, and DNA. (B) Quantification graph of the fold change of DTACC intensity in S2 cells from A. ds-*egfp*, “1” fold, n=66; ds-*hyx*, “0.75” fold, n=69. (C) Metaphase cells from S2 cells treated with ds-*egfp* (n=83) and S2 cells treated with ds-*hyx* (n=88) were analyzed with α-tub, Asl, and DNA. (D) Quantification graph of the fold change of α-tub intensity in S2 cells from C. (E) Quantification graph of the fold change of Polo intensity in S2 cells from A. ds-*egfp*, “1” fold, n=143; ds-*hyx*, “0.86” fold, n=129. (F) Spinning disc super-resolution imaging of CNN, γ-tub, and Asl in metaphase S2 cells treated with ds-*egfp* (CNN, n=46; γ-tub, n=37) and ds-*hyx* (CNN, n=39; γ-tub, n=39), respectively. (G) Quantification graph of the percentage of metaphase S2 cells forming “doughnut-like” shape of CNN and γ-tub in F. Arrows indicate the centrosomes. Scale bars: 5 μm.

Supplemental figure legends

Figure S1. Hyx regulates NSC homeostasis of *Drosophila* larval central brains.

(A) MARCM clones of control (FRT82B; n=20), *hyx*^{HT622} (n=23), and *hyx*$^{W12-46}$ (n=25) were labelled for Hyx, Dpn, and GFP. (B) Type I MARCM clones of control (FRT82B; n=20), *hyx*^{HT622} (n=17), *hyx*$^{W12-46}$ (n=30), *UAS-hyx hyx*^{HT622} (n=21), and *UAS-hyx hyx*$^{W12-46}$ (n=40) were labelled with Dpn, Ase, and CD8. Ectopic NSCs were observed in 88.2% of *hyx*^{HT622} and 36.7% of *hyx*$^{w12-46}$, but not in the control or rescued animals. (C) Type II control MARCM clones of (FRT82B), *hyx*^{HT622}, *hyx*$^{W12-46}$, *UAS-hyx hyx*^{HT622}, and *UAS-hyx hyx*$^{W12-46}$ were labelled with Dpn, Ase, and CD8. Ectopic NSCs were observed in *hyx*^{HT622} (81.0%, n=21) and *hyx*$^{w12-46}$ (78.5%, n=30), but not in control (n=20), *UAS-hyx hyx*^{HT622} (n=17) and *UAS-hyx hyx*$^{W12-46}$ (n=40). (D) MARCM clones of *UAS-HRPT2 hyx*^{HT622} type I (n=30) and type II (n=7) were labelled for Dpn, Ase, and GFP. (E) Type I and type II NSC lineages from *hyx* RNAi (V103555 with *UAS-CD8-GFP*) and *UAS-HRPT2; hyx* RNAi under the control of *insc*-Gal4 driver were labelled for Dpn, Ase, and CD8 (n=10 brain lobes for each genotype). (F) Type I (n=12) and type II (n=16) MARCM clones from *ctr9*^{12P023} were labelled for Dpn, Ase, and CD8. Clones were outlined with white dotted lines. NSCs and NSC-like cells are pointed by arrows. Scale bars: 5 μm.

Figure S2. Hyx governs asymmetric cell division of NSCs.

(A) INP lineages of control (*UAS-Dicer2*) and *hyx* RNAi (KK/V103555 with *UAS-Dicer2*) driven by *erm*-Gal4, *UAS-CD8-GFP* were labelled with Dpn, Ase, and CD8 (n=30 for both). (B) Metaphase NSCs of control (*insc>CD8-GFP*; n=50) and *hyx* RNAi (GD/V28318 with *UAS-CD8-GFP*) type II lineages were labeled with aPKC, Mira, CD8, and DNA. *hyx* RNAi: aPKC delocalization, 100%, n=50; Mira delocalization, 70%, n=50. (C) Metaphase NSCs from control (*insc>CD8-GFP*) and *hyx* RNAi (KK/V103555 with *UAS-CD8-GFP*) type II lineages were labeled with aPKC, Mira, CD8, and DNA. Delocalization of aPKC: 100% in *hyx* RNAi; Mira: 90% in *hyx* RNAi; n=50 for all. (D) Metaphase NSCs from control (*insc>CD8-GFP*) and *hyx* RNAi (GD/V28318 with *UAS-CD8-GFP*) type II lineages were labeled with Insc, Numb, CD8, and DNA. 100% delocalization of Insc and Numb in *hyx* RNAi; n=50 for all. (E) Metaphase NSCs from control (*insc>CD8-GFP*) and *hyx* RNAi (GD/V28318 with *UAS-CD8-GFP*) type II lineages were labeled with Baz, CD8, and DNA; 100% delocalization of Baz in *hyx* RNAi; n=50 for both genotypes. (F) Metaphase NSCs from control (*insc>CD8-GFP*) and *hyx* RNAi (GD/V28318 with *UAS-CD8-GFP*) type II lineages were labeled with Par6, CD8, and DNA. *hyx* RNAi: Par6 delocalization, 100%; n=50 for both genotypes. (G) Metaphase NSCs from control (*insc>CD8-GFP*) and *hyx* RNAi (GD/V28318 with *UAS-CD8-GFP*) type II lineages were labeled with Pins, CD8, and DNA. *hyx* RNAi: Pins delocalization, 100%; n=50 for both genotypes. (H) Metaphase NSCs from control (*insc>CD8-GFP*; n=50) and *hyx* RNAi (GD/V28318 with *UAS-CD8-GFP*) type II

lineages were labeled with Brat, CD8, and DNA. *hyx* RNAi: Brat delocalization, 100%; n=50 for both genotypes. Clones are outlined by white-dotted lines. Scale bars: 5 μm.

Figure S3. Hyx is required for the formation of microtubule aster and centriole number in NSCs.

(A) Interphase NSCs from control (*UAS-β-Gal* RNAi; 100% aster formation, n=20) and *hyx* RNAi (KK/V103555; n=22) were labelled for α-tub, Asl, and PH3. (B) Interphase NSCs of control (*UAS-β-Gal* RNAi; n=23) and *hyx* RNAi (KK/V103555; n=20) were analyzed with Sas-4, Asl, and PH3. (C) Prometa/metaphase NSCs of control (*UAS-β-Gal* RNAi) and *hyx* RNAi (KK/V103555) were analyzed with Sas-4, Asl, and PH3 (n=23 for both). (D) Metaphase NSCs of control (FRT82B; n=54) and hyx^{HT622} (n=37) were labelled with Asl, Msps, GFP, and PH3. Zoom-in areas are boxed. (E) Quantification graph showing the percentage of metaphase NSCs with indicated number of Asl per NSC in (D) and hyx^{w12-46} (n=8). (F) Quantification graph showing the percentage of metaphase NSCs from control (*UAS-β-Gal* RNAi; n=31) and *hyx* RNAi (KK/V103555; n=23) with indicated number of Asl. (G) Metaphase ds-*egfp*-treated S2 cells (n=195) and ds-*hyx*-treated S2 cells (n=172) were analyzed with Msps and Asl. (H) Quantification graph displaying the percentage of metaphase S2 cells with the indicated number of Asl per NSC in G. *hyx* knockdown was driven by *insc*-Gal4 in A-C. NSCs are circled by dotted lines. Arrows indicate the centrosomes. Scale bars: 5 μm.

Figure S4. Hyx is required for the recruitment of PCM proteins γ-tub and CNN to the centrosome in NSCs.

(A) Control (*UAS-β-Gal* RNAi; n=36) and *hyx* RNAi (KK/V103555; n=42) interphase NSCs were labelled for γ-tub, Asl, GFP, and PH3. (B) Control (*UAS-β-Gal* RNAi; n=25) and *hyx* RNAi (KK/V103555; n=32) metaphase NSCs were labelled for γ-tub, Asl, GFP, and PH3. In control, γ-tub robust distribution was seen in 88.9% of interphase (A) and 92.0% of metaphase (B) NSCs. (C) Quantification graph of the fold change of γ-tub intensity in NSCs from A and B. Interphase: control, “1” fold, n=36; *hyx* RNAi, “0.32” fold, n=42. Metaphase: control, “1” fold, n=25; *hyx* RNAi, “0.38” fold, n=32. (D) Interphase NSCs of control (FRT82B; n=51) and hyx^{HT622} (n=33) MARCM clones were labelled for CNN, Asl, GFP, and PH3. (E) Metaphase MARCM clones of control (FRT82B; all NSCs have robust CNN localization, n=27) and hyx^{HT622} (n=29), were analyzed by CNN, Asl, GFP, and PH3. (F) Quantification graph of the fold change of CNN intensity in NSCs from D and E. Interphase: control, “1” fold, n=51; hyx^{HT622}, “0.09” fold, n=33; hyx^{w12-46}, “0.14” fold, n=12. Metaphase: control, “1” fold, n=27; hyx^{HT622}, “0.44” fold, n=29; hyx^{w12-46}, “0.59” fold, n=18. (G) Interphase NSCs from control (*UAS-β-Gal* RNAi; 96.3% robust CNN signal) and *hyx* RNAi (KK/V103555) were labelled with CNN, Asl, GFP, and DNA (n=27 for both). (H) Metaphase NSCs of control (*UAS-β-Gal*

RNAi; 100% CNN robust localization, n=24) and *hyx* RNAi (KK/V103555; n=30) were labelled with CNN, Asl, GFP, and DNA. (I) Quantification graph of the fold change of CNN intensity in NSCs from G and H. Interphase: control, “1” fold, n=27; *hyx* RNAi, “0.13” fold, n=27. Metaphase: control, “1” fold, n=24; *hyx* RNAi, “0.74” fold, n=30. *hyx* knockdown was driven by *insc*-Gal4 in A-I. NSCs are circled by dotted lines. Arrows indicate the centrosomes. Scale bars: 5 μm.

Figure S5. Msps and D-TACC were delocalized from the centrosomes upon *hyx* depletion in NSCs.

(A) Interphase NSCs of control (*UAS-β-Gal* RNAi) and *hyx* RNAi (KK/V103555) were labelled with Msps, Asl, and PH3. Msps delocalization at the centrosomes: control: 0%, n=55; *hyx* RNAi, 82.5%, n=57. (B) Metaphase NSCs of control (*UAS-β-Gal* RNAi) and *hyx* RNAi (KK/V103555) were labelled with Msps, Asl, and PH3. Msps at the centrosomes: control: 98.5%, n=55; *hyx* RNAi, 16.4%, n=67. (C) Quantification graph of the fold change of Msps intensity in NSCs from A and B. Interphase: control, “1” fold, n=25; *hyx* RNAi, “0.07” fold, n=25. Metaphase: control, “1” fold, n=25; *hyx* RNAi, “0.10” fold, n=26. (D) Interphase NSCs from control (FRT82B; n=41) and hyx^{HT622} (n=25) MARCM clones were labelled with DTACC, Asl, GFP, and PH3. (E) MARCM clones of control (FRT82B; 100% D-TACC localization, n=18) and hyx^{HT622} (n=21) were labelled with DTACC, Asl, GFP, and PH3. (F) Quantification graph of the fold change of DTACC intensity in NSCs from D and E. Interphase: control, “1” fold, n=21; hyx^{HT622}, “0.13” fold, n=25; hyx^{w12-46}, “0.22” fold, n=22. Metaphase: control, “1” fold, n=18; hyx^{HT622}, “0.06”, n=21; hyx^{w12-46}, “0.15” fold, n=15). (G) Interphase NSCs of control (*UAS-β-Gal* RNAi) and *hyx* RNAi (KK/V103555) were examined with DTACC, Asl, and PH3. DTACC delocalization at the centrosomes: control, 3.8%, n=26; *hyx* RNAi, 83.3%, n=24. (H) Metaphase NSCs of control (*UAS-β-Gal* RNAi) and *hyx* RNAi (KK/V103555) were examined with DTACC, Asl, and PH3. DTACC delocalization at the centrosomes: control, 3.3%, n=30; *hyx* RNAi, 85.3%, n=34. (I) Quantification graph of the fold change of DTACC intensity in NSCs from G and H. Interphase: control, “1” fold, n=26; *hyx* RNAi, “0.13”, n=24. Metaphase: control, “1” fold, n=30; *hyx* RNAi, “0.20”, n=34. *hyx* knockdown was driven by *insc*-Gal4 in A-B and G-H. NSCs are circled by white-dotted lines. Centrosomes are pointed by arrows. Scale bars: 5 μm.

Figure S6. Polo and AurA were delocalized from the centrosomes upon *hyx* knockdown in NSCs and S2 cells.

(A) Interphase NSCs of control (*UAS-β-Gal* RNAi; n=29) and *hyx* RNAi (KK/V103555; n=26) were labelled with Polo, Asl, and PH3. (B) Metaphase NSCs of control (*UAS-β-Gal* RNAi; Polo present at the centrosomes in 95.0% of NSCs, n=20) and *hyx* RNAi (KK/V103555; n=23) were labelled for Polo, Asl, and DNA. (C) Quantification graph showing the fold change of Polo intensity in A and B. Interphase: control, “1” fold, n=29; *hyx* RNAi, “0.12” fold, n=26. Metaphase: control, “1” fold, n=20; *hyx* RNAi, “0.26” fold, n=24. (D) Interphase NSCs of control (*UAS-β-Gal* RNAi; AurA present at the

centrosomes in 96.6% of NSCs, n=29) and *hyx* RNAi (KK/V103555; n=24) were labelled with AurA, Asl, GFP, and PH3. (E) Metaphase NSCs of control (*UAS-β-Gal* RNAi; AurA observed at the centrosomes in 96.4% of NSCs, n=28) and *hyx* RNAi (KK/V103555; n=30) were analyzed with AurA, Asl, GFP, and PH3. Polo localization and AurA are properly localized in all control NSCs in A-E. (F) Quantification graph showing the fold change of AurA intensity in D and E. Interphase: control, “1” fold, n=29; *hyx* RNAi, “0.04” fold, n=24. Metaphase: control, “1” fold, n=28; *hyx* RNAi, “0.53” fold, n=30. (G) Metaphase cells from ds-*egfp*-treated S2 cells and ds-*hyx*-treated S2 cells were analyzed with Ana2, γ-tub, and DNA. (H) Quantification graph showed the fold change of Ana2 intensity in G. ds-*egfp*, “1” fold, n=38; ds-*hyx*, “0.83” fold, n=30. (I) Quantification graph showing the fold change of γ-tub intensity in G. ds-*egfp*, “1” fold, n=69; ds-*hyx*, “1.03” fold, n=52. *hyx* knockdown was under the control of *insc*-Gal4 in A-F. NSCs are outlined by white-dotted lines. Centrosomes are pointed by arrows. Scale bars: 5 μm.

Movie S1. Time-lapse imaging of G147/+ (Jupiter-GFP) NSCs under the control of *insc*-Gal4 at 48h ALH larval brains. Time scale: minute: second. Scale bar: 5 μm.

Movie S2. Time-lapse imaging of *hyx* RNAi (KK/V103555); G147 NSCs under the control of *insc*-Gal4 at 48h ALH larval brains. Time scale: minute: second. Scale bar: 5 μm.

REFERENCES

Agarwal, S. K., W. F. Simonds and S. J. Marx (2008). "The parafibromin tumor suppressor protein interacts with actin-binding proteins actinin-2 and actinin-3." Molecular cancer **7**: 65-65.

Atwood, S. X., C. Chabu, R. R. Penkert, C. Q. Doe and K. E. Prehoda (2007). "Cdc42 acts downstream of Bazooka to regulate neuroblast polarity through Par-6 aPKC." Journal of cell science **120**(Pt 18): 3200-3206.

Bahrampour, S. and S. Thor (2016). "Ctr9, a Key Component of the Paf1 Complex, Affects Proliferation and Terminal Differentiation in the Developing Drosophila Nervous System." G3: Genes|Genomes|Genetics **6**(10): 3229.

Bello, B., H. Reichert and F. Hirth (2006). "The brain tumor gene negatively regulates neural progenitor cell proliferation in the larval central brain of Drosophila." Development **133**(14): 2639-2648.

Bello, B. C., N. Izergina, E. Caussinus and H. Reichert (2008). "Amplification of neural stem cell proliferation by intermediate progenitor cells in Drosophila brain development." Neural Develop **3**: 5.

Berdnik, D. and J. A. Knoblich (2002). "Drosophila Aurora-A Is Required for Centrosome Maturation and Actin-Dependent Asymmetric Protein Localization during Mitosis." Current Biology **12**(8): 640-647.

Betschinger, J., K. Mechtler and J. A. Knoblich (2006). "Asymmetric Segregation of the Tumor Suppressor Brat Regulates Self-Renewal in Drosophila Neural Stem Cells." Cell **124**(6): 1241-1253.

Boone, J. Q. and C. Q. Doe (2008). "Identification of Drosophila type II neuroblast lineages containing transit amplifying ganglion mother cells." Dev Neurobiol **68**(9): 1185-1195.

Bowman, S. K., R. A. Neumüller, M. Novatchkova, Q. Du and J. A. Knoblich (2006). "The Drosophila NuMA Homolog Mud regulates spindle orientation in asymmetric cell division." Dev Cell **10**(6): 731-742.

Bowman, S. K., V. Rolland, J. Betschinger, K. A. Kinsey, G. Emery and J. A. Knoblich (2008). "The tumor suppressors Brat and Numb regulate transit-amplifying neuroblast lineages in Drosophila." Dev Cell **14**(4): 535-546.

Caussinus, E. and C. Gonzalez (2005). "Induction of tumor growth by altered stem-cell asymmetric division in Drosophila melanogaster." Nat Genet **37**(10): 1125-1129.

Chabu, C. and C. Q. Doe (2009). "Twins/PP2A regulates aPKC to control neuroblast cell polarity and self-renewal." Developmental Biology **330**(2): 399-405.

Chang, K. C., C. Wang and H. Wang (2012). "Balancing self-renewal and differentiation by asymmetric division: insights from brain tumor suppressors in Drosophila neural stem cells." Bioessays **34**(4): 301-310.

Chaturvedi, D., M. Inaba, S. Scoggin and M. Buszczak (2016). "Drosophila CG2469 Encodes a Homolog of Human CTR9 and Is Essential for Development." G3 (Bethesda) **6**(12): 3849-3857.

Chen, K., C. T. Koe, Z. B. Xing, X. Tian, F. Rossi, C. Wang, Q. Tang, W. Zong, W. J.

Hong, R. Taneja, F. Yu, C. Gonzalez, C. Wu, S. Endow and H. Wang (2016). "Arl2- and Msps-dependent microtubule growth governs asymmetric division." Journal of Cell Biology **212**(6): 661-676.
Choksi, S. P., T. D. Southall, T. Bossing, K. Edoff, E. de Wit, Bettina E. Fischer, B. van Steensel, G. Micklem and A. H. Brand (2006). "Prospero Acts as a Binary Switch between Self-Renewal and Differentiation in Drosophila Neural Stem Cells." Developmental Cell **11**(6): 775-789.
Doe, C. Q. (2008). "Neural stem cells: balancing self-renewal with differentiation." Development **135**(9): 1575-1587.
Doe, C. Q. (2008). "Neural stem cells: balancing self-renewal with differentiation." Development **135**(9): 1575-1587.
Dzhindzhev, N. S., Q. D. Yu, K. Weiskopf, G. Tzolovsky, I. Cunha-Ferreira, M. Riparbelli, A. Rodrigues-Martins, M. Bettencourt-Dias, G. Callaini and D. M. Glover (2010). "Asterless is a scaffold for the onset of centriole assembly." Nature **467**(7316): 714-718.
Gartenmann, L., C. C. Vicente, A. Wainman, Z. A. Novak, B. Sieber, J. H. Richens and J. W. Raff (2020). "Drosophila Sas-6, Ana2 and Sas-4 self-organise into macromolecular structures that can be used to probe centriole and centrosome assembly." Journal of Cell Science **133**(12).
Giet, R., D. McLean, S. Descamps, M. J. Lee, J. W. Raff, C. Prigent and D. M. Glover (2002). "Drosophila Aurora A kinase is required to localize D-TACC to centrosomes and to regulate astral microtubules." J Cell Biol **156**(3): 437-451.
Giet, R., D. McLean, S. Descamps, M. J. Lee, J. W. Raff, C. Prigent and D. M. Glover (2002). "Drosophila Aurora A kinase is required to localize D-TACC to centrosomes and to regulate astral microtubules." The Journal of cell biology **156**(3): 437-451.
Gonzalez, C. (2007). "Spindle orientation, asymmetric division and tumour suppression in Drosophila stem cells." Nat Rev Genet **8**(6): 462-472.
Hannaford, M. R., A. Ramat, N. Loyer and J. Januschke (2018). "aPKC-mediated displacement and actomyosin-mediated retention polarize Miranda in Drosophila neuroblasts." eLife **7**: e29939.
Ikeshima-Kataoka, H., J. B. Skeath, Y.-i. Nabeshima, C. Q. Doe and F. Matsuzaki (1997). "Miranda directs Prospero to a daughter cell during Drosophila asymmetric divisions." Nature **390**(6660): 625-629.
Izumi, Y., N. Ohta, K. Hisata, T. Raabe and F. Matsuzaki (2006). "Drosophila Pins-binding protein Mud regulates spindle-polarity coupling and centrosome organization." Nat Cell Biol **8**(6): 586-593.
Januschke, J. and C. Gonzalez (2008). "Drosophila asymmetric division, polarity and cancer." Oncogene **27**(55): 6994-7002.
Januschke, J. and C. Gonzalez (2010). "The interphase microtubule aster is a determinant of asymmetric division orientation in Drosophila neuroblasts." Journal of Cell Biology **188**(5): 693-706.
Jo, J.-H., T.-M. Chung, H. Youn and J.-Y. Yoo (2014). "Cytoplasmic parafibromin/hCdc73 targets and destabilizes p53 mRNA to control p53-mediated

apoptosis." Nature Communications **5**(1): 5433.
Kelsom, C. and W. Lu (2012). "Uncovering the link between malfunctions in Drosophila neuroblast asymmetric cell division and tumorigenesis." Cell & Bioscience **2**(1): 38.
Knoblich, J. A. (2010). "Asymmetric cell division: recent developments and their implications for tumour biology." Nat Rev Mol Cell Biol **11**(12): 849-860.
Koe, C. T. and H. Wang Asymmetric Cell Division in Drosophila Neuroblasts. eLS**:** 1-14.
Krahn, M. P., D. Egger-Adam and A. Wodarz (2009). "PP2A Antagonizes Phosphorylation of Bazooka by PAR-1 to Control Apical-Basal Polarity in Dividing Embryonic Neuroblasts." Developmental Cell **16**(6): 901-908.
Kraut, R., W. Chia, L. Y. Jan, Y. N. Jan and J. A. Knoblich (1996). "Role of inscuteable in orienting asymmetric cell divisions in Drosophila." Nature **383**(6595): 50-55.
Kubota, Y., K. Tsuyama, Y. Takabayashi, N. Haruta, R. Maruyama, N. Iida and A. Sugimoto (2014). "The PAF1 complex is involved in embryonic epidermal morphogenesis in Caenorhabditis elegans." Developmental Biology **391**(1): 43-53.
Lee, C.-Y., R. O. Andersen, C. Cabernard, L. Manning, K. D. Tran, M. J. Lanskey, A. Bashirullah and C. Q. Doe (2006). "Drosophila Aurora-A kinase inhibits neuroblast self-renewal by regulating aPKC/Numb cortical polarity and spindle orientation." Genes & Development **20**(24): 3464-3474.
Lee, C.-Y., K. J. Robinson and C. Q. Doe (2006). "Lgl, Pins and aPKC regulate neuroblast self-renewal versus differentiation." Nature **439**(7076): 594-598.
Lee, C.-Y., B. D. Wilkinson, S. E. Siegrist, R. P. Wharton and C. Q. Doe (2006). "Brat Is a Miranda Cargo Protein that Promotes Neuronal Differentiation and Inhibits Neuroblast Self-Renewal." Developmental Cell **10**(4): 441-449.
Lee, C. Y., R. O. Andersen, C. Cabernard, L. Manning, K. D. Tran, M. J. Lanskey, A. Bashirullah and C. Q. Doe (2006). "Drosophila Aurora-A kinase inhibits neuroblast self-renewal by regulating aPKC/Numb cortical polarity and spindle orientation." Genes Dev **20**(24): 3464-3474.
Lee, M. J., F. Gergely, K. Jeffers, S. Y. Peak-Chew and J. W. Raff (2001). "Msps/XMAP215 interacts with the centrosomal protein D-TACC to regulate microtubule behaviour." Nature Cell Biology **3**(7): 643-649.
Lee, T. and L. Luo (1999). "Mosaic analysis with a repressible cell marker for studies of gene function in neuronal morphogenesis." Neuron **22**(3): 451-461.
Li, S., C. T. Koe, S. T. Tay, A. L. K. Tan, S. Zhang, Y. Zhang, P. Tan, W.-K. Sung and H. Wang (2017). "An intrinsic mechanism controls reactivation of neural stem cells by spindle matrix proteins." Nature Communications **8**(1).
Lin, L., J. H. Zhang, L. M. Panicker and W. F. Simonds (2008). "The parafibromin tumor suppressor protein inhibits cell proliferation by repression of the c-myc proto-oncogene." Proc Natl Acad Sci U S A **105**(45): 17420-17425.
Lu, B., M. Rothenberg, L. Y. Jan and Y. N. Jan (1998). "Partner of Numb colocalizes with Numb during mitosis and directs Numb asymmetric localization in Drosophila neural and muscle progenitors." Cell **95**(2): 225-235.
Ly, P. T., Y. S. Tan, C. T. Koe, Y. Zhang, G. Xie, S. Endow, W. M. Deng, F. Yu and H. Wang (2019). "CRL4Mahj E3 ubiquitin ligase promotes neural stem cell reactivation."

PLoS Biol **17**(6): e3000276.
Matsuzaki, F., T. Ohshiro, H. Ikeshima-Kataoka and H. Izumi (1998). "miranda localizes staufen and prospero asymmetrically in mitotic neuroblasts and epithelial cells in early Drosophila embryogenesis." Development **125**(20): 4089-4098.
Morin, X., R. Daneman, M. Zavortink and W. Chia (2001). "A protein trap strategy to detect GFP-tagged proteins expressed from their endogenous loci in Drosophila." Proc Natl Acad Sci U S A **98**(26): 15050-15055.
Moritz, M., M. B. Braunfeld, J. W. Sedat, B. Alberts and D. A. Agard (1995). "Microtubule nucleation by gamma-tubulin-containing rings in the centrosome." Nature **378**(6557): 638-640.
Mosimann, C., G. Hausmann and K. Basler (2006). "Parafibromin/Hyrax Activates Wnt/Wg Target Gene Transcription by Direct Association with β-catenin/Armadillo." Cell **125**(2): 327-341.
Mosimann, C., G. Hausmann and K. Basler (2006). "Parafibromin/Hyrax activates Wnt/Wg target gene transcription by direct association with beta-catenin/Armadillo." Cell **125**(2): 327-341.
Mosimann, C., G. Hausmann and K. Basler (2006). "Parafibromin/Hyrax Activates Wnt/Wg Target Gene Transcription by Direct Association with β-catenin/Armadillo." Cell **125**(2): 327-341.
Mueller, C. L. and J. A. Jaehning (2002). "Ctr9, Rtf1, and Leo1 Are Components of the Paf1/RNA Polymerase II Complex." Molecular and Cellular Biology **22**(7): 1971.
Neumüller, R. A. and J. A. Knoblich (2009). "Dividing cellular asymmetry: asymmetric cell division and its implications for stem cells and cancer." Genes & Development **23**(23): 2675-2699.
Neumüller, R. A., C. Richter, A. Fischer, M. Novatchkova, K. G. Neumüller and J. A. Knoblich (2011). "Genome-wide analysis of self-renewal in Drosophila neural stem cells by transgenic RNAi." Cell stem cell **8**(5): 580-593.
Newey, P. J., M. R. Bowl and R. V. Thakker (2009). "Parafibromin--functional insights." J Intern Med **266**(1): 84-98.
Novak, Zsofia A., A. Wainman, L. Gartenmann and Jordan W. Raff (2016). "Cdk1 Phosphorylates Drosophila Sas-4 to Recruit Polo to Daughter Centrioles and Convert Them to Centrosomes." Developmental Cell **37**(6): 545-557.
Ogawa, H., N. Ohta, W. Moon and F. Matsuzaki (2009). "Protein phosphatase 2A negatively regulates aPKC signaling by modulating phosphorylation of Par-6 in Drosophila neuroblast asymmetric divisions." J Cell Sci **122**(Pt 18): 3242-3249.
Petronczki, M. and J. A. Knoblich (2001). "DmPAR-6 directs epithelial polarity and asymmetric cell division of neuroblasts in Drosophila." Nature Cell Biology **3**(1): 43-49.
Porzionato, A., V. Macchi, L. Barzon, G. Masi, M. Iacobone, A. Parenti, G. Palu and R. De Caro (2006). "Immunohistochemical assessment of parafibromin in mouse and human tissues." J Anat **209**(6): 817-827.
Porzionato, A., V. Macchi, L. Barzon, G. Masi, M. Iacobone, A. Parenti, G. Palù and R. De Caro (2006). "Immunohistochemical assessment of parafibromin in mouse and human tissues." Journal of anatomy **209**(6): 817-827.
Rea, S., F. Eisenhaber, D. O'Carroll, B. D. Strahl, Z. W. Sun, M. Schmid, S. Opravil, K.

Mechtler, C. P. Ponting, C. D. Allis and T. Jenuwein (2000). "Regulation of chromatin structure by site-specific histone H3 methyltransferases." Nature **406**(6796): 593-599.
Roth, S. and R. Heintzmann (2016). "Optical photon reassignment with increased axial resolution by structured illumination." Methods and Applications in Fluorescence **4**(4): 045005.
Rusan, N. M. and M. Peifer (2007). "A role for a novel centrosome cycle in asymmetric cell division." The Journal of cell biology **177**(1): 13-20.
Schaefer, M., M. Petronczki, D. Dorner, M. Forte and J. A. Knoblich (2001). "Heterotrimeric G Proteins Direct Two Modes of Asymmetric Cell Division in the Drosophila Nervous System." Cell **107**(2): 183-194.
Schober, M., M. Schaefer and J. A. Knoblich (1999). "Bazooka recruits Inscuteable to orient asymmetric cell divisions in Drosophila neuroblasts." Nature **402**(6761): 548-551.
Selvarajan, S., L. H. Sii, A. Lee, G. Yip, B. H. Bay, M. H. Tan, B. T. Teh and P. H. Tan (2008). "Parafibromin expression in breast cancer: a novel marker for prognostication?" J Clin Pathol **61**(1): 64-67.
Shen, C.-P., L. Y. Jan and Y. N. Jan (1997). "Miranda Is Required for the Asymmetric Localization of Prospero during Mitosis in Drosophila." Cell **90**(3): 449-458.
Sunkel, C. E., R. Gomes, P. Sampaio, J. Perdigão and C. González (1995). "Gamma-tubulin is required for the structure and function of the microtubule organizing centre in Drosophila neuroblasts." The EMBO journal **14**(1): 28-36.
Terada, Y., Y. Uetake and R. Kuriyama (2003). "Interaction of Aurora-A and centrosomin at the microtubule-nucleating site in Drosophila and mammalian cells." The Journal of cell biology **162**(5): 757-763.
Varmark, H., S. Llamazares, E. Rebollo, B. Lange, J. Reina, H. Schwarz and C. Gonzalez (2007). "Asterless Is a Centriolar Protein Required for Centrosome Function and Embryo Development in Drosophila." Current Biology **17**(20): 1735-1745.
Wang, C., K. C. Chang, G. Somers, D. Virshup, B. T. Ang, C. Tang, F. Yu and H. Wang (2009). "Protein phosphatase 2A regulates self-renewal of Drosophila neural stem cells." Development **136**(13): 2287.
Wang, C., K. C. Chang, G. Somers, D. Virshup, B. T. Ang, C. Tang, F. Yu and H. Wang (2009). "Protein phosphatase 2A regulates self-renewal of Drosophilaneural stem cells." Development **136**(13): 2287-2296.
Wang, C., S. Li, J. Januschke, F. Rossi, Y. Izumi, G. Garcia-Alvarez, S. S. Gwee, S. B. Soon, H. K. Sidhu, F. Yu, F. Matsuzaki, C. Gonzalez and H. Wang (2011). "An ana2/ctp/mud complex regulates spindle orientation in Drosophila neuroblasts." Dev Cell **21**(3): 520-533.
Wang, C., S. Li, J. Januschke, F. Rossi, Y. Izumi, G. Garcia-Alvarez, Serene Sze L. Gwee, Swee B. Soon, Harpreet K. Sidhu, F. Yu, F. Matsuzaki, C. Gonzalez and H. Wang (2011). "An Ana2/Ctp/Mud Complex Regulates Spindle Orientation in Drosophila Neuroblasts." Developmental Cell **21**(3): 520-533.
Wang, G., Q. Jiang and C. Zhang (2014). "The role of mitotic kinases in coupling the centrosome cycle with the assembly of the mitotic spindle." J Cell Sci **127**(Pt 19): 4111-

4122.
Wang, H., Y. Ouyang, W. G. Somers, W. Chia and B. Lu (2007). "Polo inhibits progenitor self-renewal and regulates Numb asymmetry by phosphorylating Pon." Nature **449**(7158): 96-100.
Wang, H., G. W. Somers, A. Bashirullah, U. Heberlein, F. Yu and W. Chia (2006). "Aurora-A acts as a tumor suppressor and regulates self-renewal of Drosophila neuroblasts." Genes Dev **20**(24): 3453-3463.
Wang, H., G. W. Somers, A. Bashirullah, U. Heberlein, F. Yu and W. Chia (2006). "Aurora-A acts as a tumor suppressor and regulates self-renewal of Drosophila neuroblasts." Genes & Development **20**(24): 3453-3463.
Wang, P., M. R. Bowl, S. Bender, J. Peng, L. Farber, J. Chen, A. Ali, Z. Zhang, A. S. Alberts, R. V. Thakker, A. Shilatifard, B. O. Williams and B. T. Teh (2008). "Parafibromin, a component of the human PAF complex, regulates growth factors and is required for embryonic development and survival in adult mice." Molecular and cellular biology **28**(9): 2930-2940.
Wei, Y., L. Yu, J. Bowen, M. A. Gorovsky and C. D. Allis (1999). "Phosphorylation of histone H3 is required for proper chromosome condensation and segregation." Cell **97**(1): 99-109.
Weng, M., K. L. Golden and C. Y. Lee (2010). "dFezf/Earmuff maintains the restricted developmental potential of intermediate neural progenitors in Drosophila." Dev Cell **18**(1): 126-135.
Wodarz, A., A. Ramrath, A. Grimm and E. Knust (2000). "Drosophila atypical protein kinase C associates with Bazooka and controls polarity of epithelia and neuroblasts." The Journal of cell biology **150**(6): 1361-1374.
Wodarz, A., A. Ramrath, U. Kuchinke and E. Knust (1999). "Bazooka provides an apical cue for Inscuteable localization in Drosophila neuroblasts." Nature **402**(6761): 544-547.
Woodard, G. E., L. Lin, J. H. Zhang, S. K. Agarwal, S. J. Marx and W. F. Simonds (2005). "Parafibromin, product of the hyperparathyroidism-jaw tumor syndrome gene HRPT2, regulates cyclin D1/PRAD1 expression." Oncogene **24**(7): 1272-1276.
Wu, P.-S., B. Egger and A. H. Brand (2008). "Asymmetric stem cell division: Lessons from Drosophila." Seminars in Cell & Developmental Biology **19**(3): 283-293.
Yang, Y.-J., J.-W. Han, H.-D. Youn and E.-J. Cho (2010). "The tumor suppressor, parafibromin, mediates histone H3 K9 methylation for cyclin D1 repression." Nucleic acids research **38**(2): 382-390.
Yu, F., X. Morin, Y. Cai, X. Yang and W. Chia (2000). "Analysis of partner of inscuteable, a Novel Player of Drosophila Asymmetric Divisions, Reveals Two Distinct Steps in Inscuteable Apical Localization." Cell **100**(4): 399-409.
Yu, F., H. Wang, H. Qian, R. Kaushik, M. Bownes, X. Yang and W. Chia (2005). "Locomotion defects, together with Pins, regulates heterotrimeric G-protein signaling during Drosophila neuroblast asymmetric divisions." Genes & development **19**(11): 1341-1353.
Zhang, Z., X. F. Yang, K. Q. Huang, L. Ren, W. F. Gou, D. F. Shen, S. Zhao, H. Z. Sun, Y. Takano and H. C. Zheng (2015). "The clinicopathological significances and biological

functions of parafibromin expression in head and neck squamous cell carcinomas." Tumour Biol **36**(12): 9487-9497.
Zheng, H. C., H. Takahashi, X. H. Li, T. Hara, S. Masuda, Y. F. Guan and Y. Takano (2008). "Downregulated parafibromin expression is a promising marker for pathogenesis, invasion, metastasis and prognosis of gastric carcinomas." Virchows Arch **452**(2): 147-155.
Zhu, B., S. S. Mandal, A.-D. Pham, Y. Zheng, H. Erdjument-Bromage, S. K. Batra, P. Tempst and D. Reinberg (2005). "The human PAF complex coordinates transcription with events downstream of RNA synthesis." Genes & Development **19**(14): 1668-1673.

Fig 1

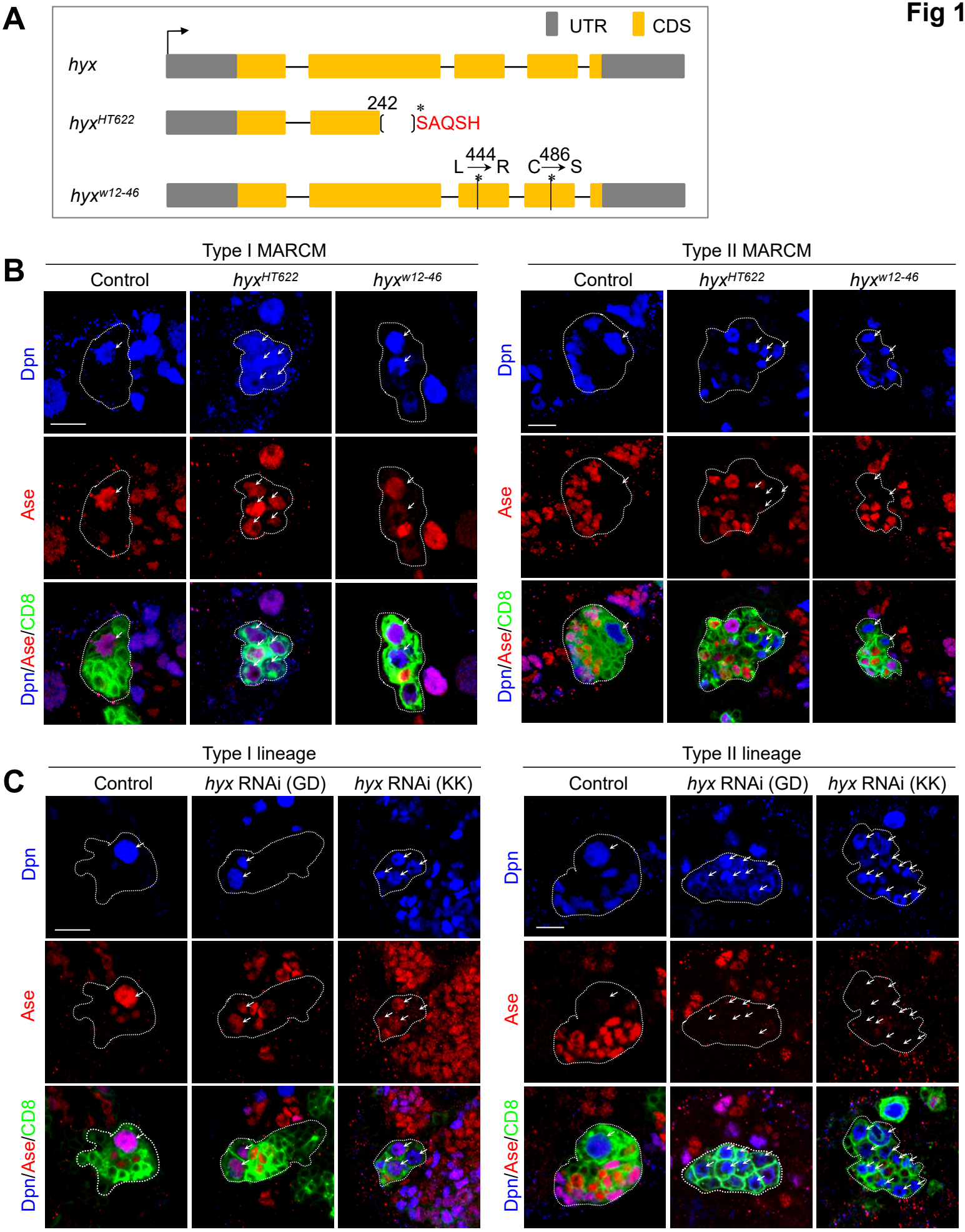
A
UTR
CDS
hyx
hyxHT622
242
SAQSH
hyxw12-46
L 444 R
C 486 S
B
Type I MARCM
Type II MARCM
Control
hyxHT622
hyxw12-46
Dpn
Ase
Dpn/Ase/CD8
C
Type I lineage
Type II lineage
Control
hyx RNAi (GD)
hyx RNAi (KK)
Dpn
Ase
Dpn/Ase/CD8

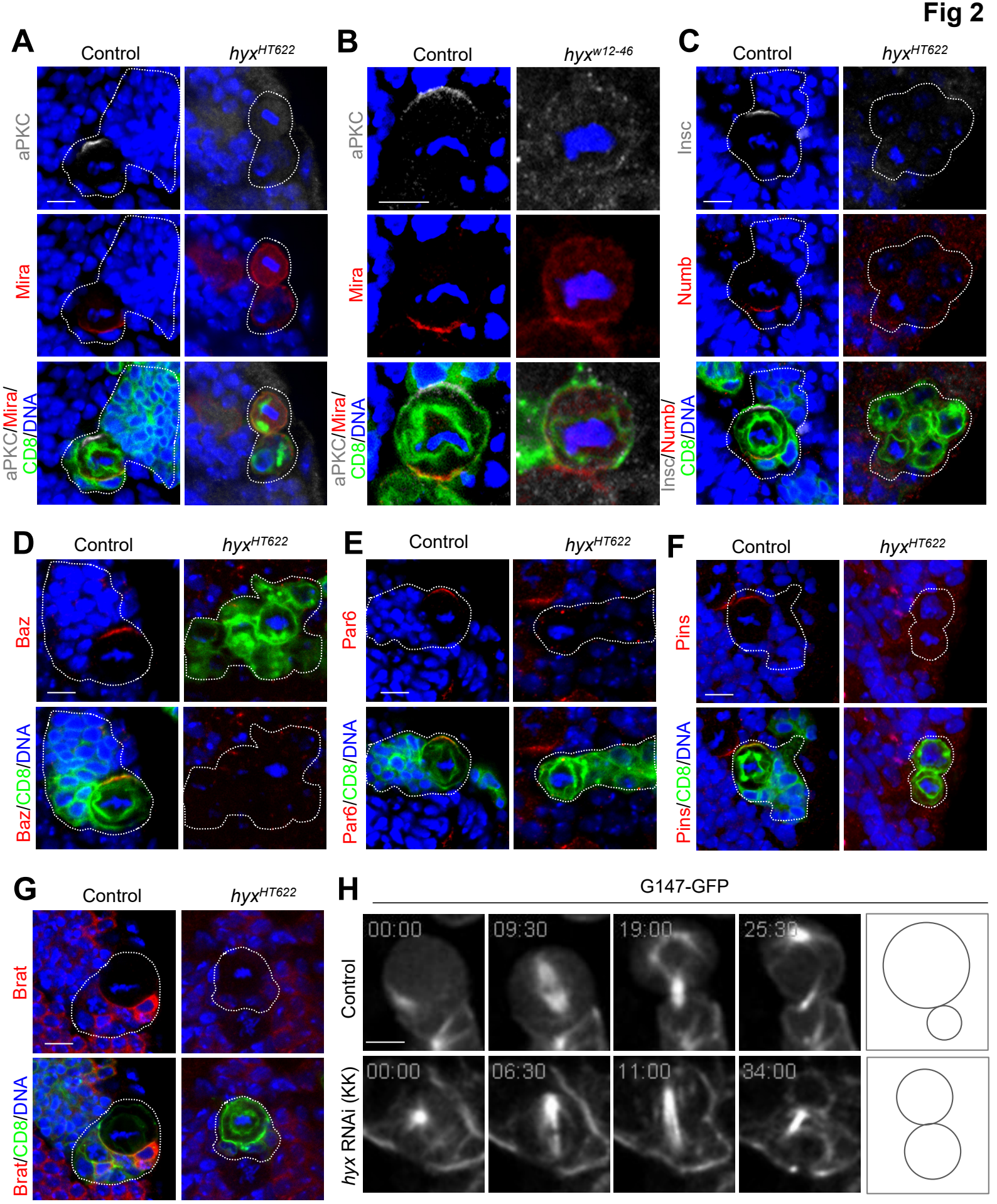
Fig 2
A
Control
hyxHT622
aPKC
Mira
aPKC/Mira/
CD8/DNA
B
Control
hyxw12-46
aPKC
Mira
aPKC/Mira/
CD8/DNA
C
Control
hyxHT622
Insc
Numb
Insc/Numb/
CD8/DNA
D
Control
hyxHT622
Baz
Baz/CD8/DNA
E
Control
hyxHT622
Par6
Par6/CD8/DNA
F
Control
hyxHT622
Pins
Pins/CD8/DNA
G
Control
hyxHT622
Brat
Brat/CD8/DNA
H
G147-GFP
Control
00:00
09:30
19:00
25:30
hyx RNAi (KK)
00:00
06:30
11:00
34:00

Fig 3

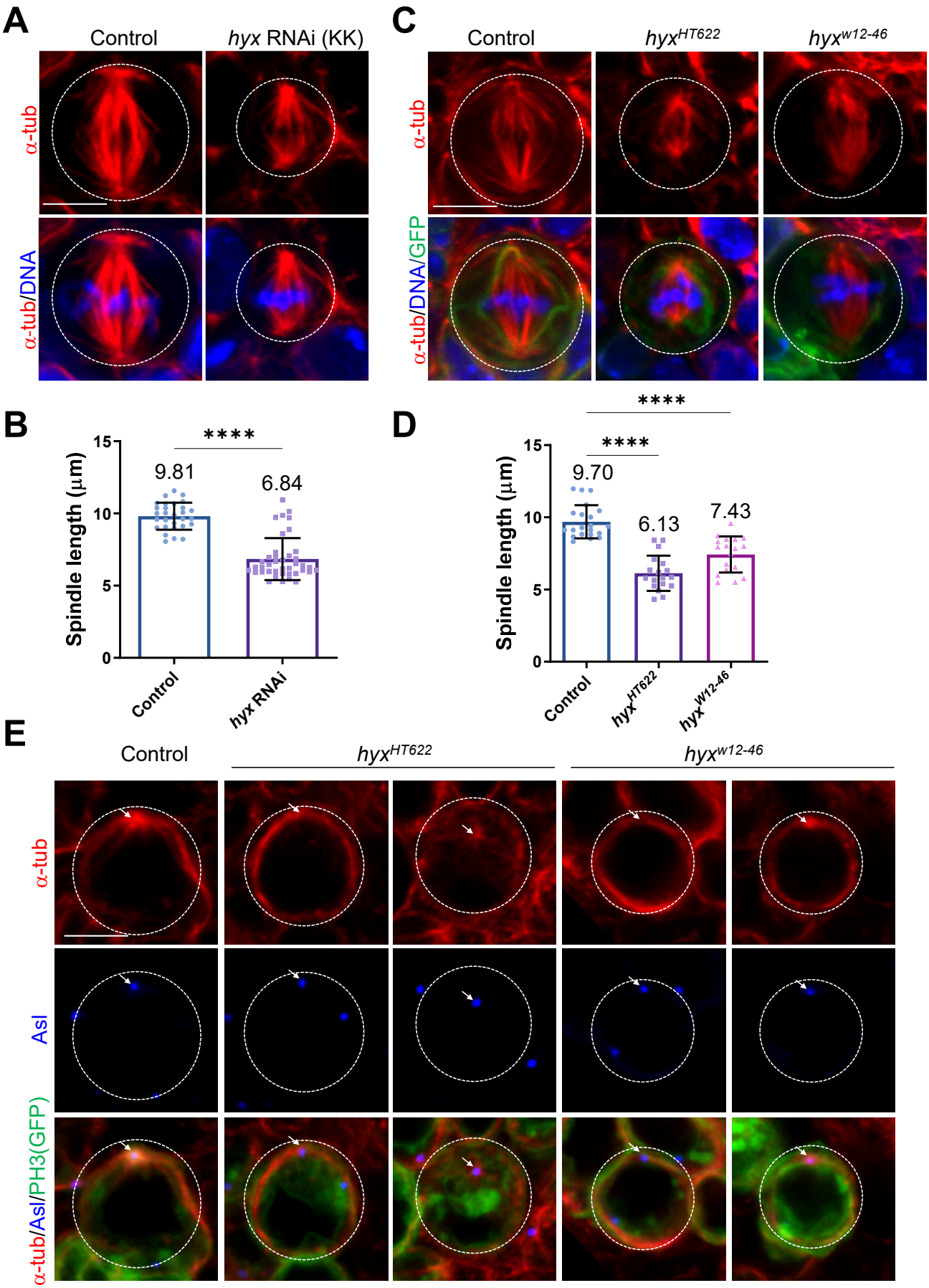
A
Control
hyx RNAi (KK)
α-tub
α-tub/DNA
B
Spindle length (μm)
****
9.81
6.84
Control
hyx RNAi
C
Control
hyxHT622
hyxw12-46
α-tub
α-tub/DNA/GFP
D
Spindle length (μm)
****
****
9.70
6.13
7.43
Control
hyxHT622
hyxW12-46
E
Control
hyxHT622
hyxw12-46
α-tub
Asl
α-tub/Asl/PH3(GFP)

Fig 4

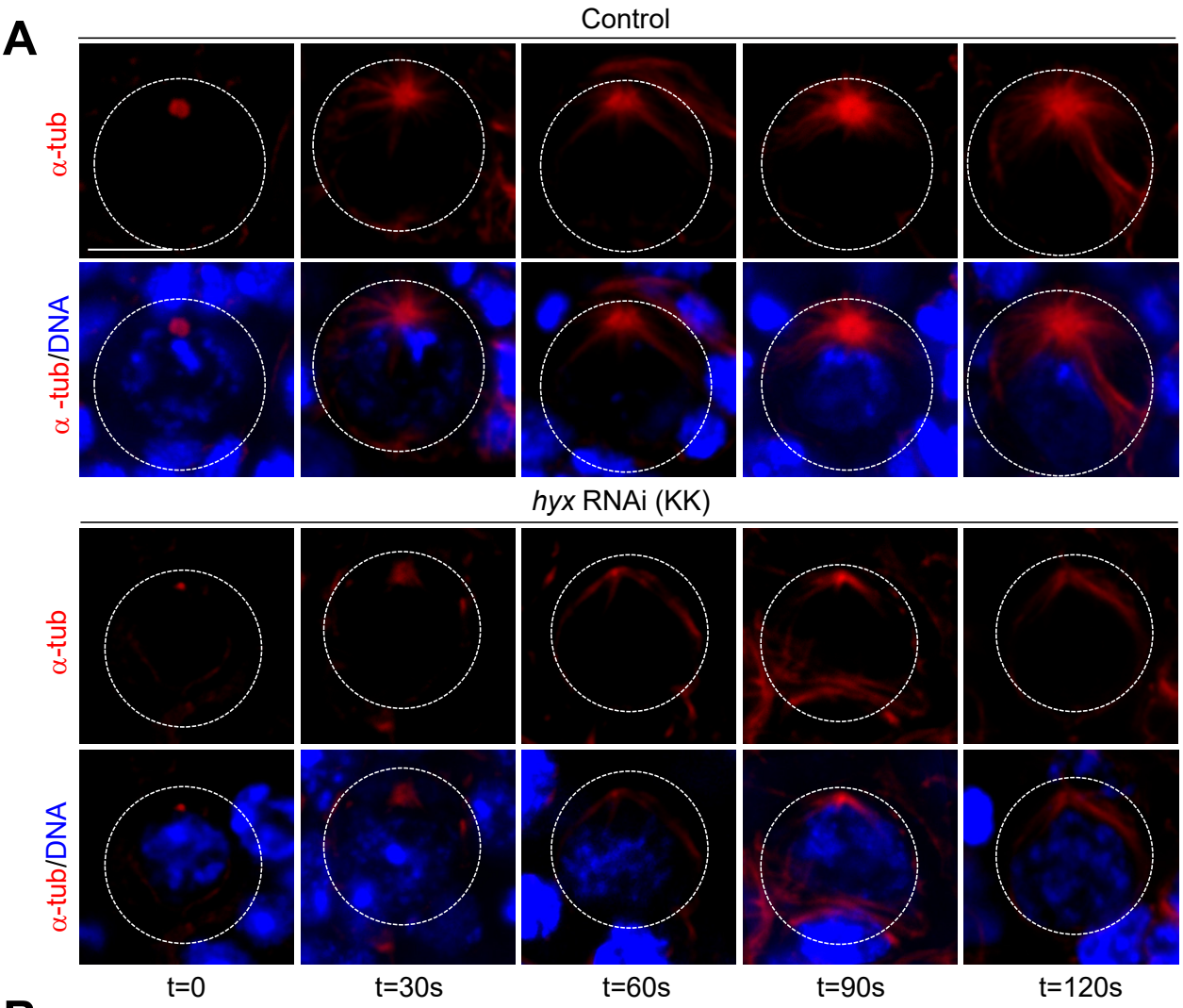
A
Control
α-tub
α -tub/DNA
hyx RNAi (KK)
α-tub
α-tub/DNA
t=0
t=30s
t=60s
t=90s
t=120s

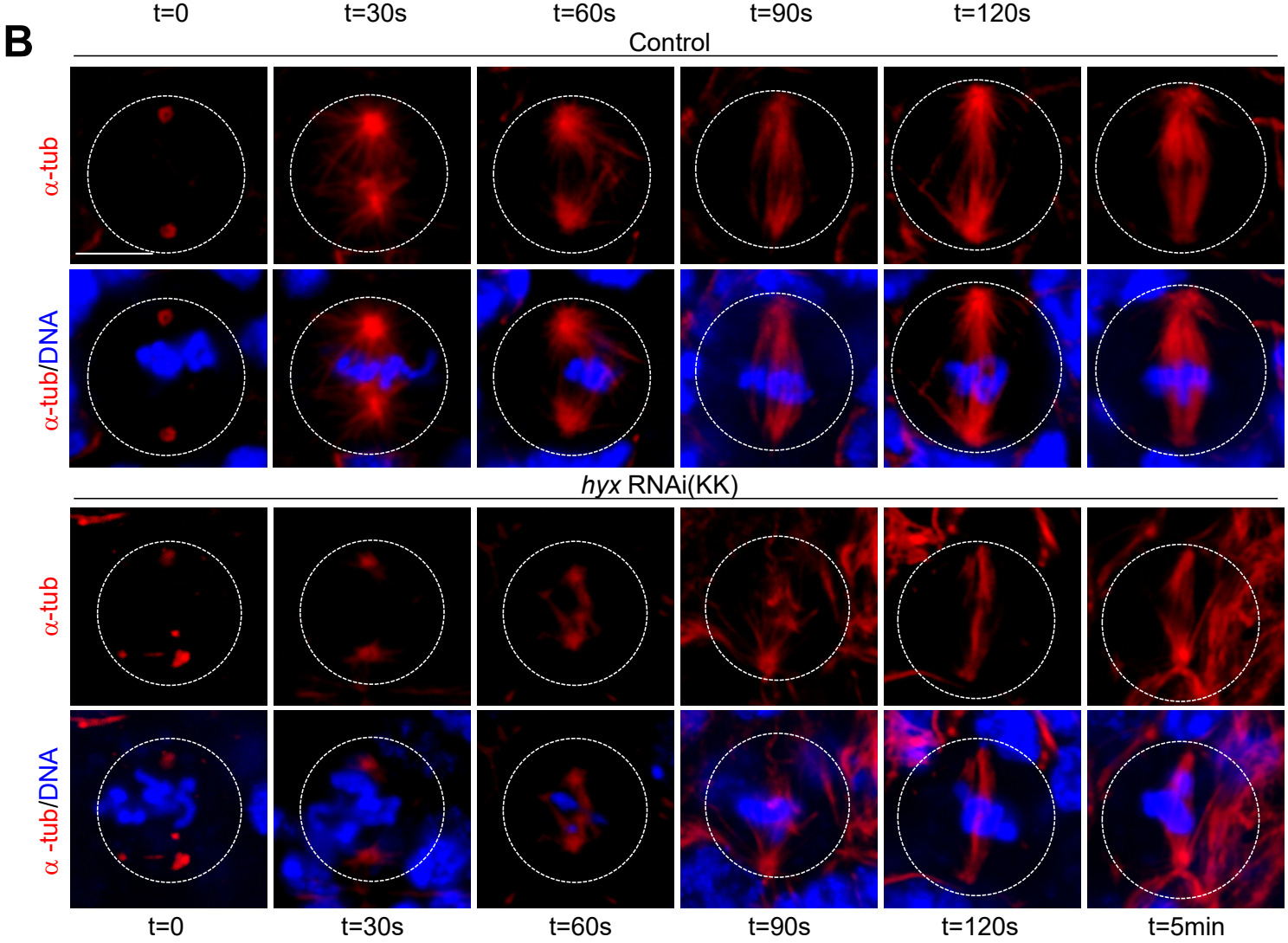
B
Control
α-tub
α-tub/DNA
hyx RNAi(KK)
α-tub
α -tub/DNA
t=0
t=30s
t=60s
t=90s
t=120s
t=5min

Fig 5

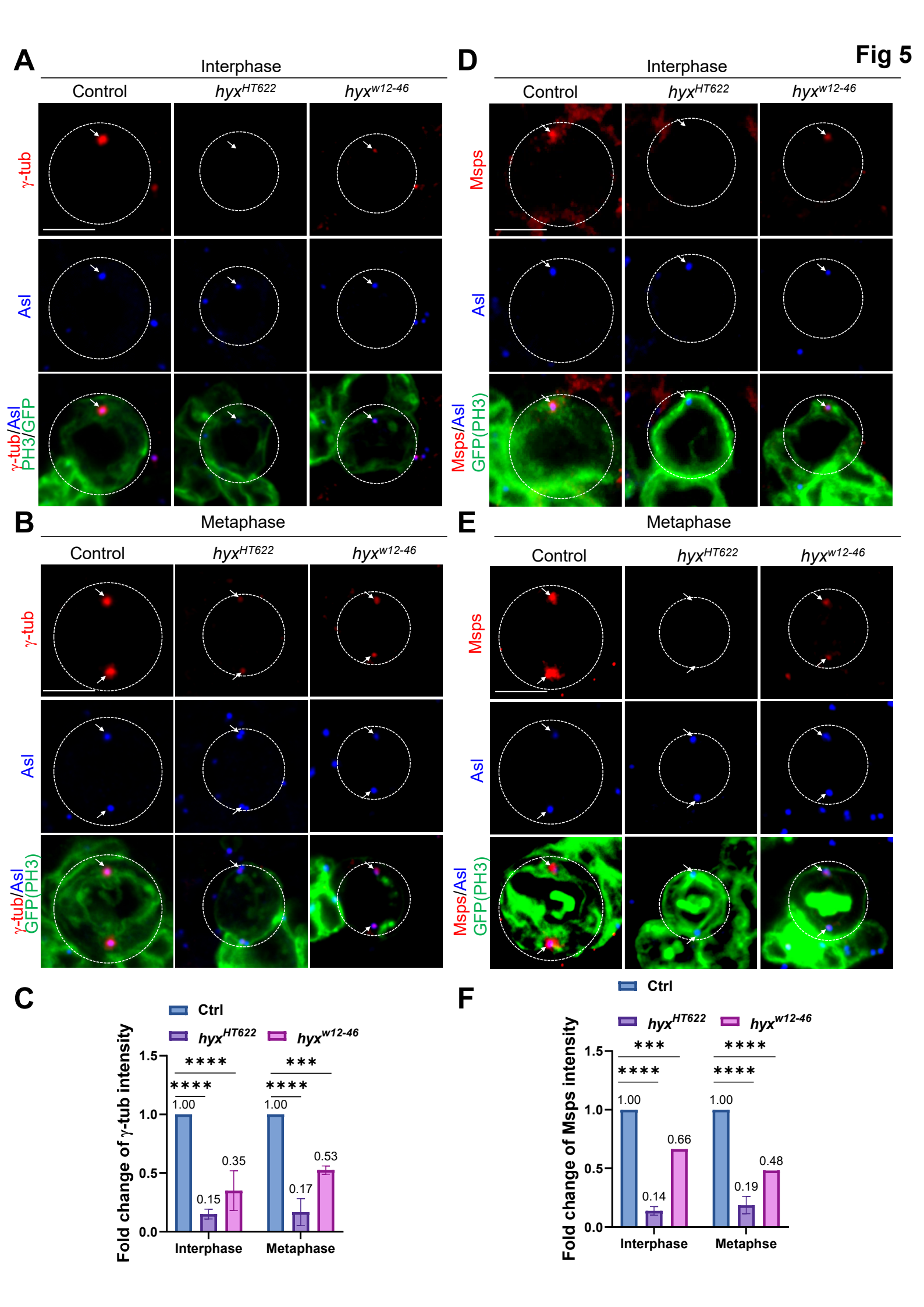
A
Interphase
Control
hyxHT622
hyxw12-46
γ-tub
Asl
γ-tub/Asl
PH3/GFP
B
Metaphase
Control
hyxHT622
hyxw12-46
γ-tub
Asl
γ-tub/Asl
GFP(PH3)
C
Ctrl
hyxHT622
hyxw12-46
Fold change of γ-tub intensity
1.5
1.0
0.5
0.0
****
****
***
****
1.00
0.15
0.35
1.00
0.17
0.53
Interphase
Metaphase
D
Interphase
Control
hyxHT622
hyxw12-46
Msps
Asl
Msps/Asl
GFP(PH3)
E
Metaphase
Control
hyxHT622
hyxw12-46
Msps
Asl
Msps/Asl
GFP(PH3)
F
Ctrl
hyxHT622
hyxw12-46
Fold change of Msps intensity
1.5
1.0
0.5
0.0
***
****
****
****
1.00
0.14
0.66
1.00
0.19
0.48
Interphase
Metaphse

Fig 6

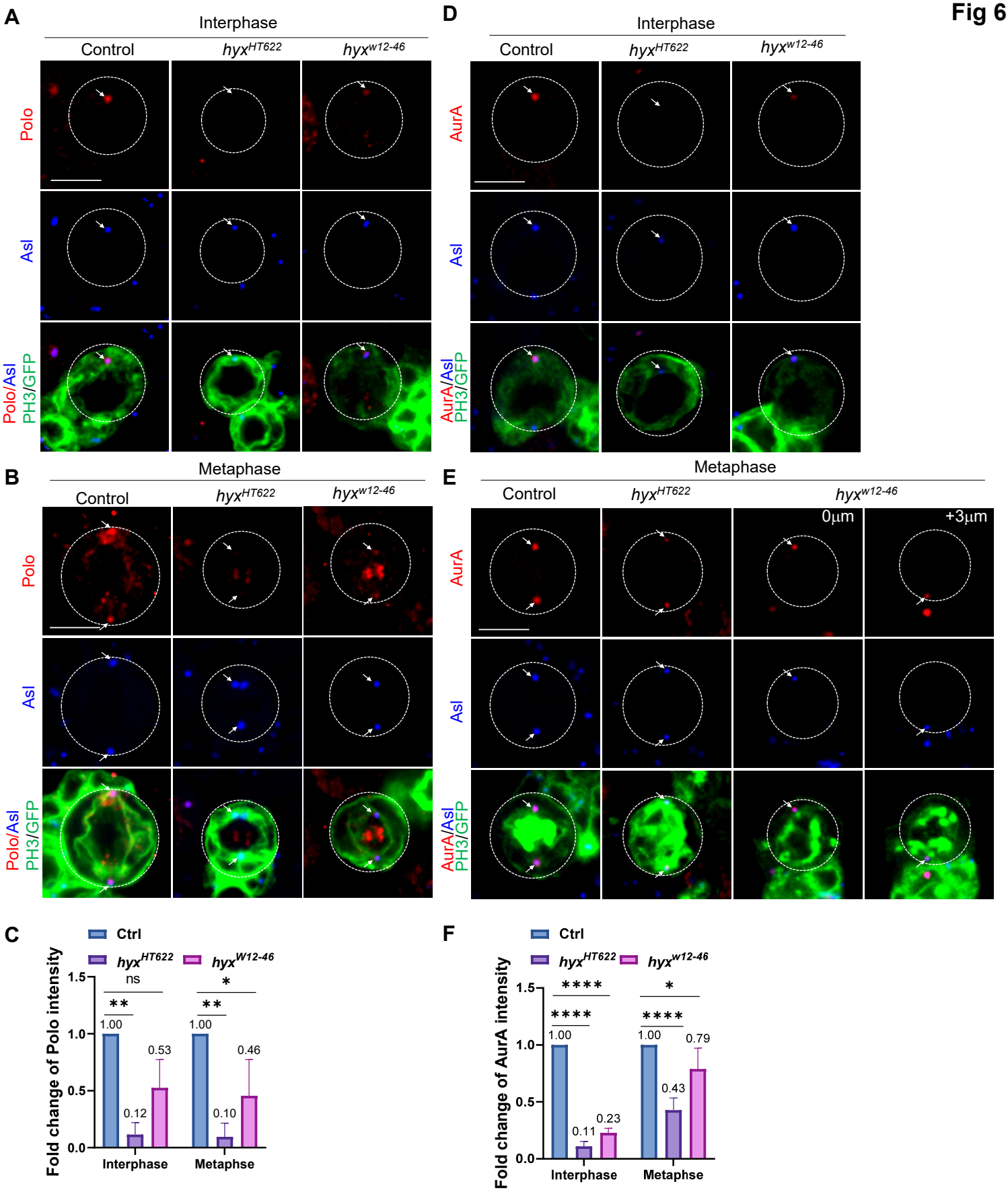
A
Interphase
Control
hyxHT622
hyxw12-46
Polo
Asl
Polo/Asl
PH3/GFP
B
Metaphase
Control
hyxHT622
hyxw12-46
Polo
Asl
Polo/Asl
PH3/GFP
C
Ctrl
hyxHT622
hyxW12-46
Fold change of Polo intensity
ns
**
*
**
1.00
0.12
0.53
1.00
0.10
0.46
1.5
1.0
0.5
0.0
Interphase
Metaphse
D
Interphase
Control
hyxHT622
hyxw12-46
AurA
Asl
AurA/Asl
PH3/GFP
E
Metaphase
Control
hyxHT622
hyxw12-46
0µm
+3µm
AurA
Asl
AurA/Asl
PH3/GFP
F
Ctrl
hyxHT622
hyxw12-46
Fold change of AurA intensity
****
****
*
****
1.00
0.11
0.23
1.00
0.43
0.79
1.5
1.0
0.5
0.0
Interphase
Metaphse

Fig 7

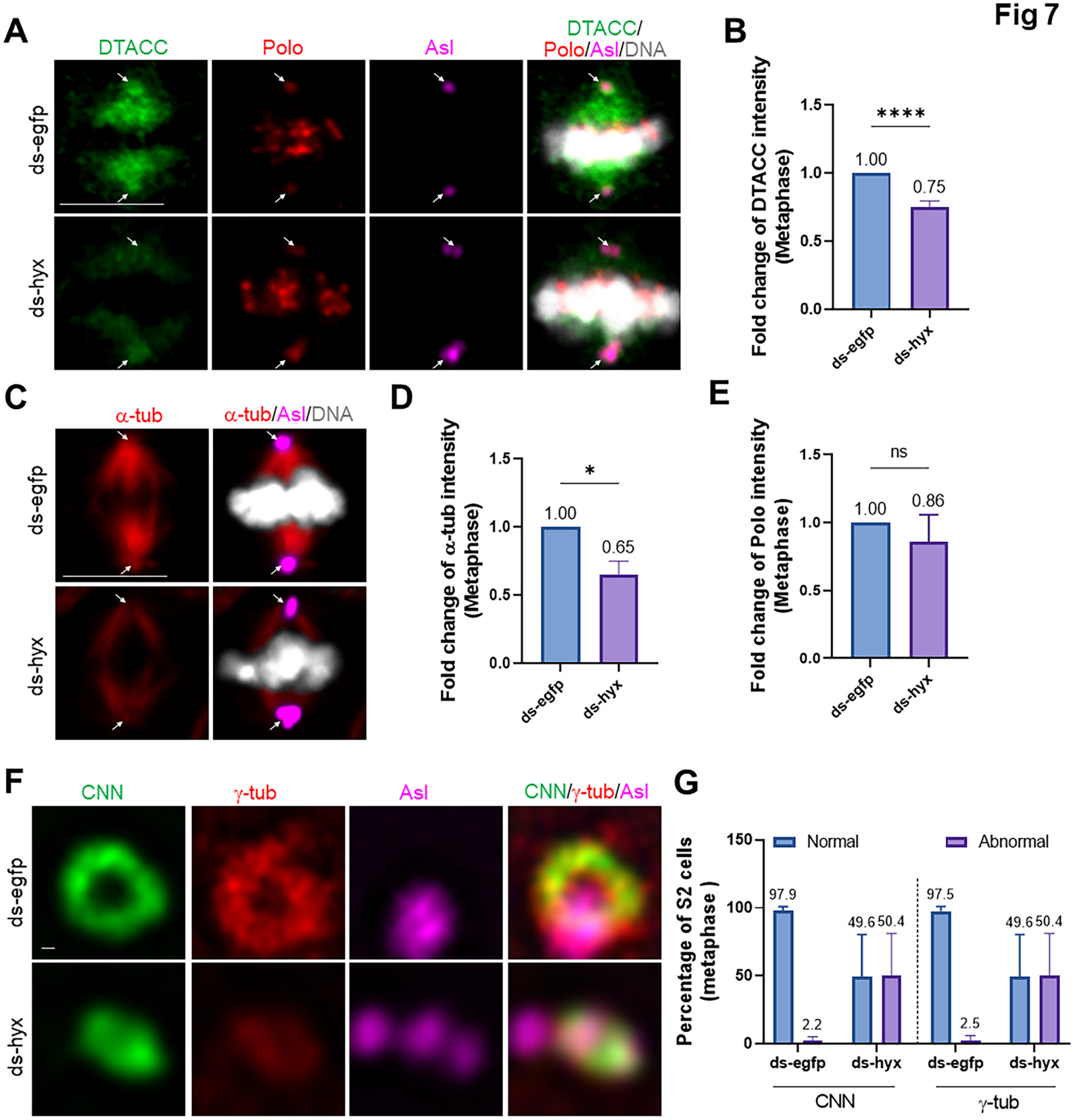
A
DTACC
Polo
Asl
DTACC/
Polo/Asl/DNA
ds-egfp
ds-hyx
B
Fold change of DTACC intensity
(Metaphase)
****
1.00
0.75
1.5
1.0
0.5
0.0
ds-egfp
ds-hyx
C
α-tub
α-tub/Asl/DNA
ds-egfp
ds-hyx
D
Fold change of α-tub intensity
(Metaphase)
*
1.00
0.65
1.5
1.0
0.5
0.0
ds-egfp
ds-hyx
E
Fold change of Polo intensity
(Metaphase)
ns
1.00
0.86
1.5
1.0
0.5
0.0
ds-egfp
ds-hyx
F
CNN
γ-tub
Asl
CNN/γ-tub/Asl
ds-egfp
ds-hyx
G
Percentage of S2 cells
(metaphase)
Normal
Abnormal
150
100
50
0
97.9
2.2
49.6
50.4
97.5
2.5
49.6
50.4
ds-egfp
ds-hyx
ds-egfp
ds-hyx
CNN
γ-tub

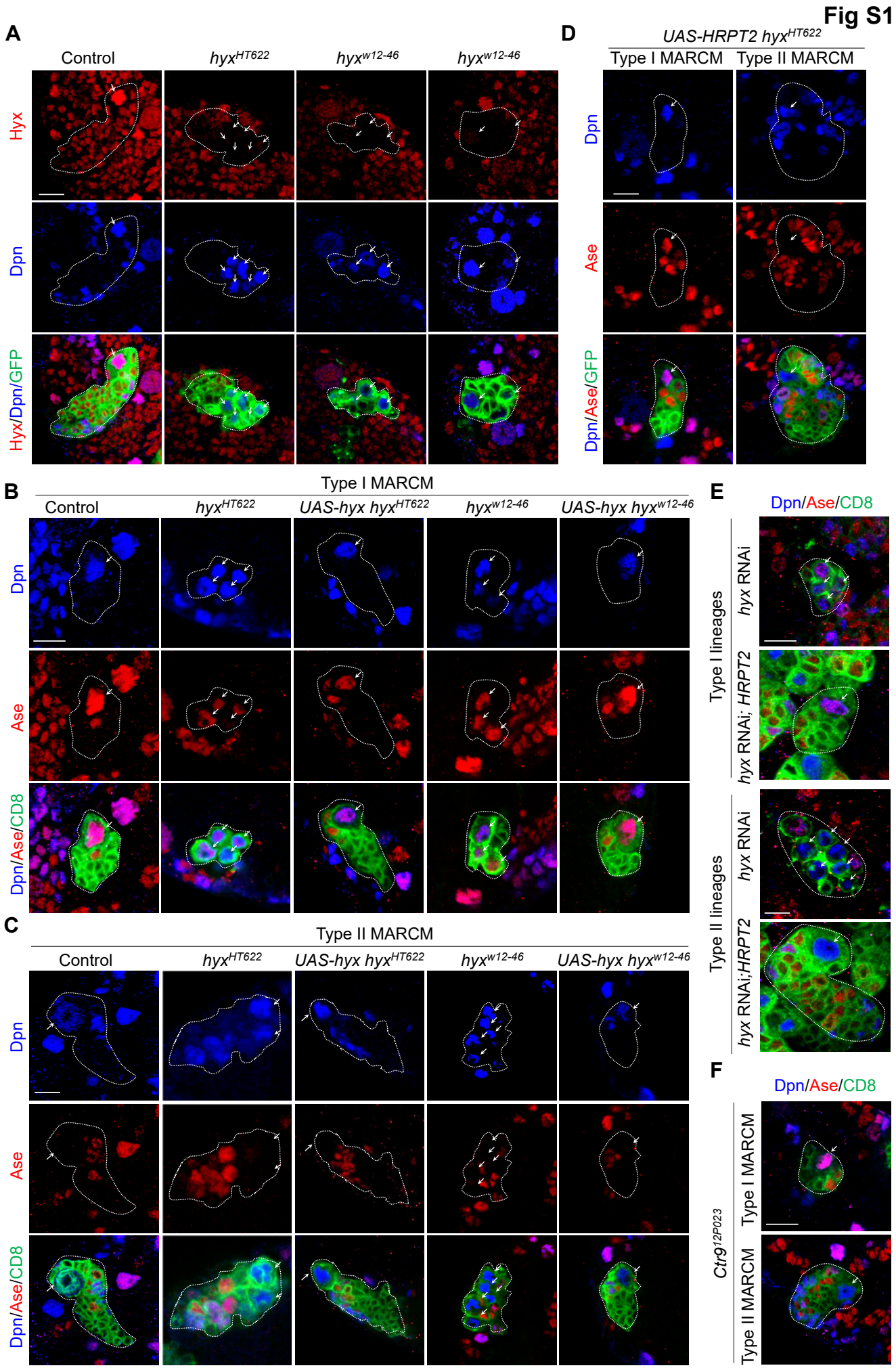
Fig S1
A
Control
hyx^HT622
hyx^w12-46
hyx^w12-46
Hyx
Dpn
Hyx/Dpn/GFP
D
UAS-HRPT2 hyx^HT622
Type I MARCM
Type II MARCM
Dpn
Ase
Dpn/Ase/GFP
B
Type I MARCM
Control
hyx^HT622
UAS-hyx hyx^HT622
hyx^w12-46
UAS-hyx hyx^w12-46
Dpn
Ase
Dpn/Ase/CD8
C
Type II MARCM
Control
hyx^HT622
UAS-hyx hyx^HT622
hyx^w12-46
UAS-hyx hyx^w12-46
Dpn
Ase
Dpn/Ase/CD8
E
Dpn/Ase/CD8
Type I lineages
hyx RNAi
hyx RNAi; HRPT2
Type II lineages
hyx RNAi
hyx RNAi;HRPT2
F
Dpn/Ase/CD8
Ctr9^12P023
Type I MARCM
Type II MARCM

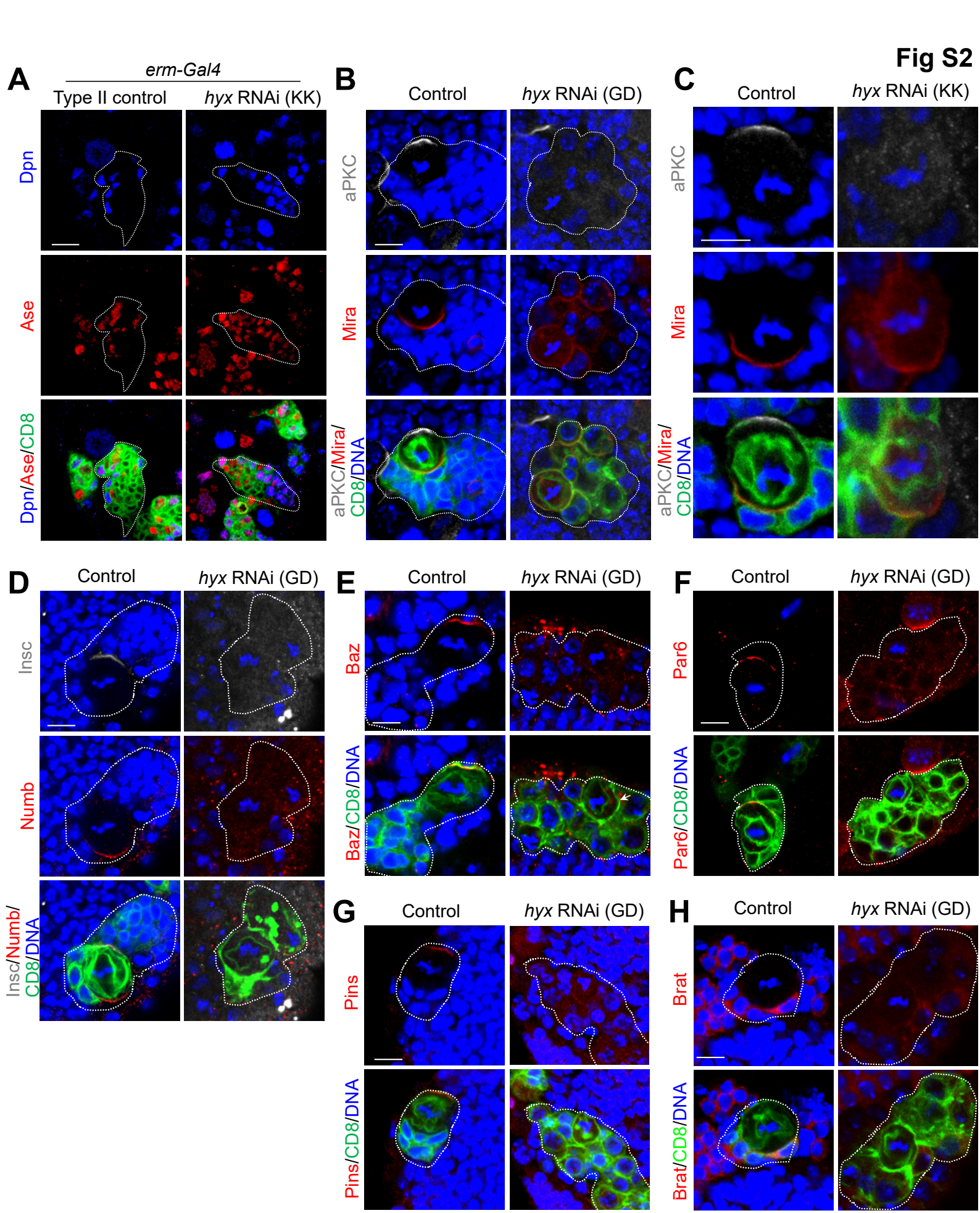
Fig S2
A
erm-Gal4
Type II control
hyx RNAi (KK)
Dpn
Ase
Dpn/Ase/CD8
B
Control
hyx RNAi (GD)
aPKC
Mira
aPKC/Mira/
CD8/DNA
C
Control
hyx RNAi (KK)
aPKC
Mira
aPKC/Mira/
CD8/DNA
D
Control
hyx RNAi (GD)
Insc
Numb
Insc/Numb/
CD8/DNA
E
Control
hyx RNAi (GD)
Baz
Baz/CD8/DNA
F
Control
hyx RNAi (GD)
Par6
Par6/CD8/DNA
G
Control
hyx RNAi (GD)
Pins
Pins/CD8/DNA
H
Control
hyx RNAi (GD)
Brat
Brat/CD8/DNA

Fig S3

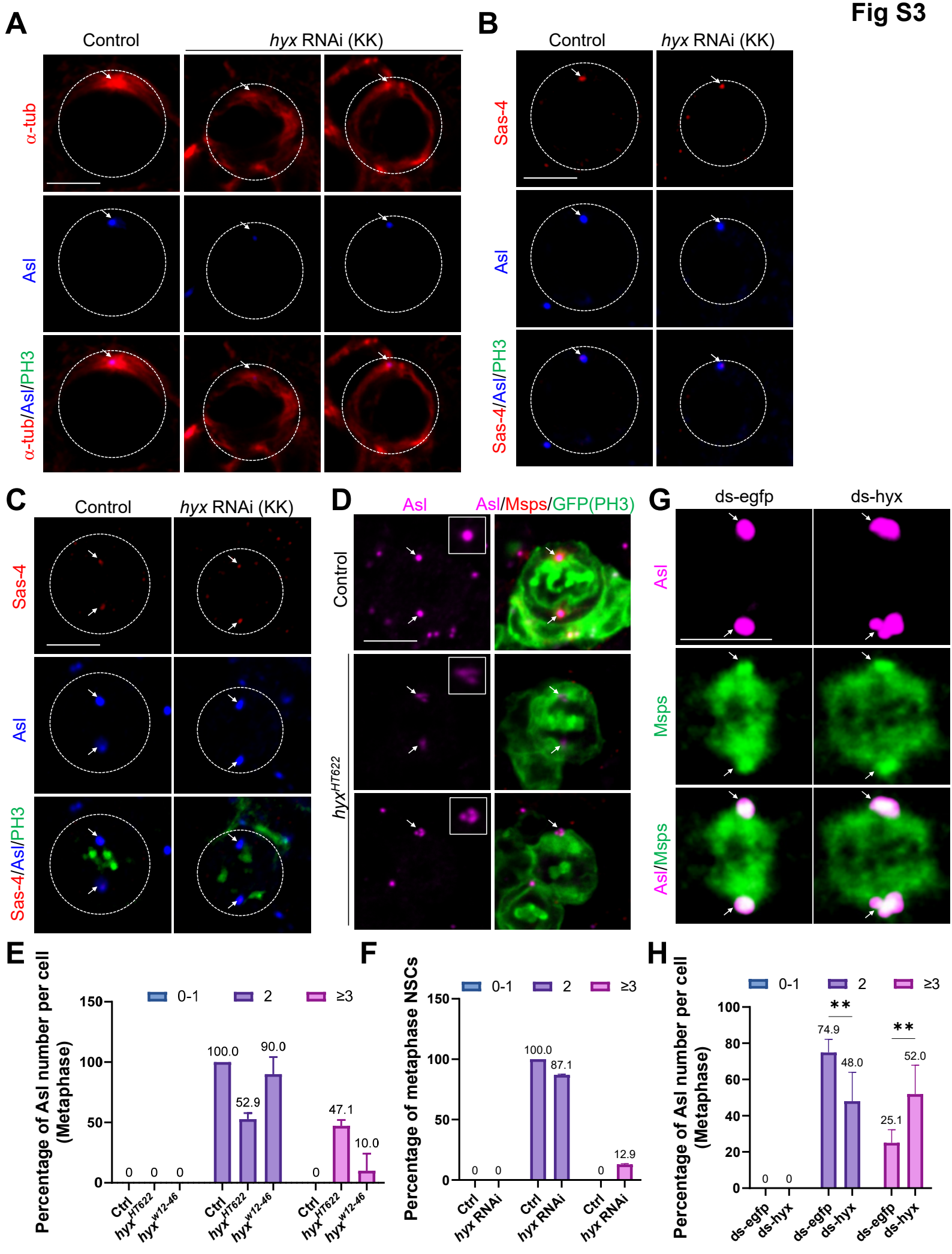
A
Control
hyx RNAi (KK)
α-tub
Asl
α-tub/Asl/PH3
B
Control
hyx RNAi (KK)
Sas-4
Asl
Sas-4/Asl/PH3
C
Control
hyx RNAi (KK)
Sas-4
Asl
Sas-4/Asl/PH3
D
Asl
Asl/Msps/GFP(PH3)
Control
hyxHT622
G
ds-egfp
ds-hyx
Asl
Msps
Asl/Msps
E
Percentage of Asl number per cell (Metaphase)
0-1
2
≥3
150
100
50
0
100.0
52.9
90.0
47.1
10.0
0
0
0
0
Ctrl
hyxHT622
hyxW12-46
F
Percentage of metaphase NSCs
0-1
2
≥3
100.0
87.1
12.9
0
0
0
Ctrl
hyx RNAi
H
Percentage of Asl number per cell (Metaphase)
0-1
2
≥3
**
**
74.9
48.0
52.0
25.1
0
0
ds-egfp
ds-hyx

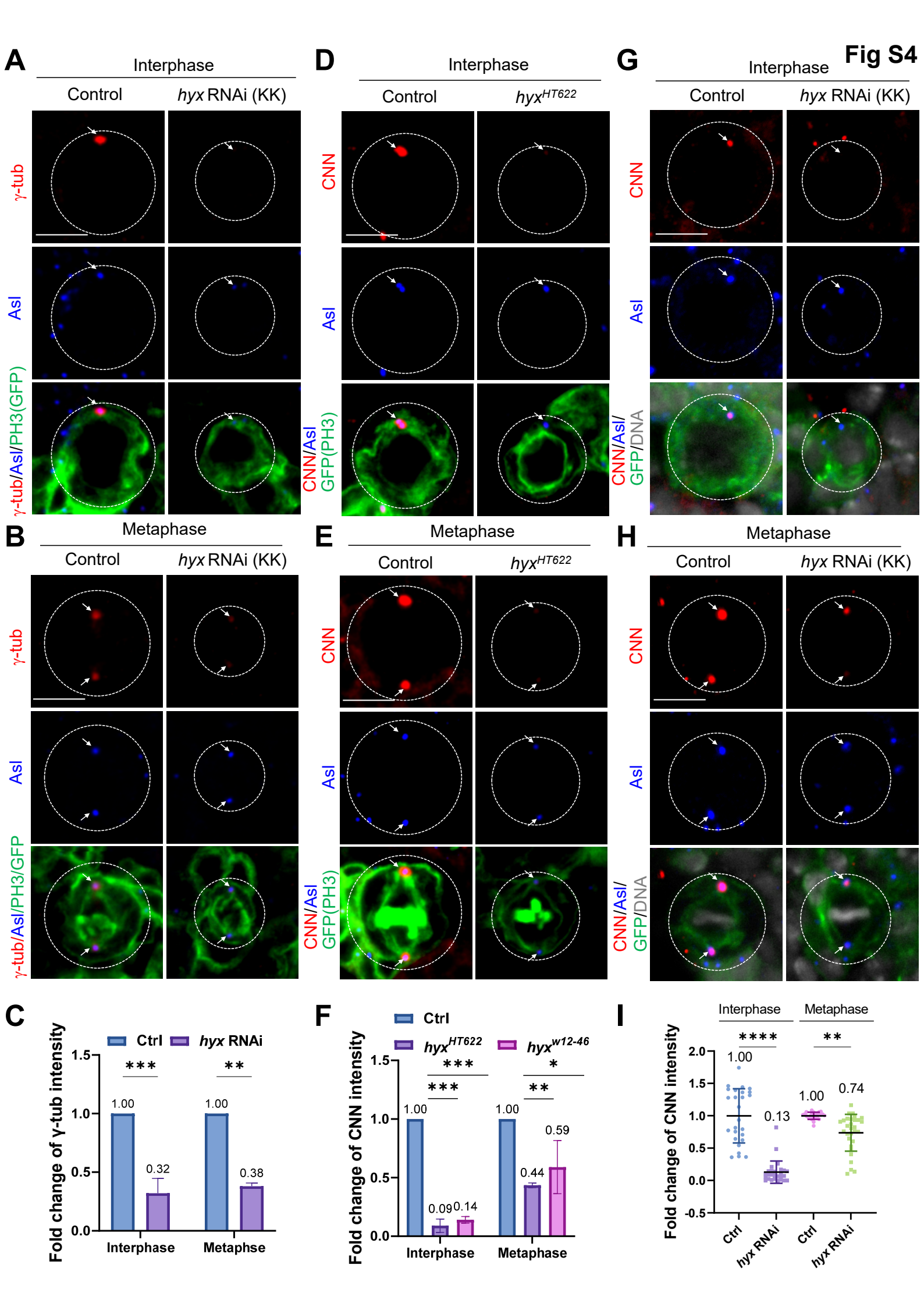
Fig S4
A
Interphase
Control
hyx RNAi (KK)
γ-tub
Asl
γ-tub/Asl/PH3(GFP)
B
Metaphase
Control
hyx RNAi (KK)
γ-tub
Asl
γ-tub/Asl/PH3/GFP
D
Interphase
Control
hyxHT622
CNN
Asl
CNN/Asl
GFP(PH3)
E
Metaphase
Control
hyxHT622
CNN
Asl
CNN/Asl
GFP(PH3)
G
Interphase
Control
hyx RNAi (KK)
CNN
Asl
CNN/Asl/
GFP/DNA
H
Metaphase
Control
hyx RNAi (KK)
CNN
Asl
CNN/Asl/
GFP/DNA
C
Ctrl
hyx RNAi
Fold change of γ-tub intensity
1.5
1.0
0.5
0.0
***
**
1.00
0.32
1.00
0.38
Interphase
Metaphse
F
Ctrl
hyxHT622
hyxw12-46
Fold change of CNN intensity
1.5
1.0
0.5
0.0
***
***
*
**
1.00
0.09
0.14
1.00
0.44
0.59
Interphase
Metaphase
I
Interphase
Metaphase
Fold change of CNN intensity
2.0
1.5
1.0
0.5
0.0
-0.5
****
**
1.00
0.13
1.00
0.74
Ctrl
hyx RNAi
Ctrl
hyx RNAi

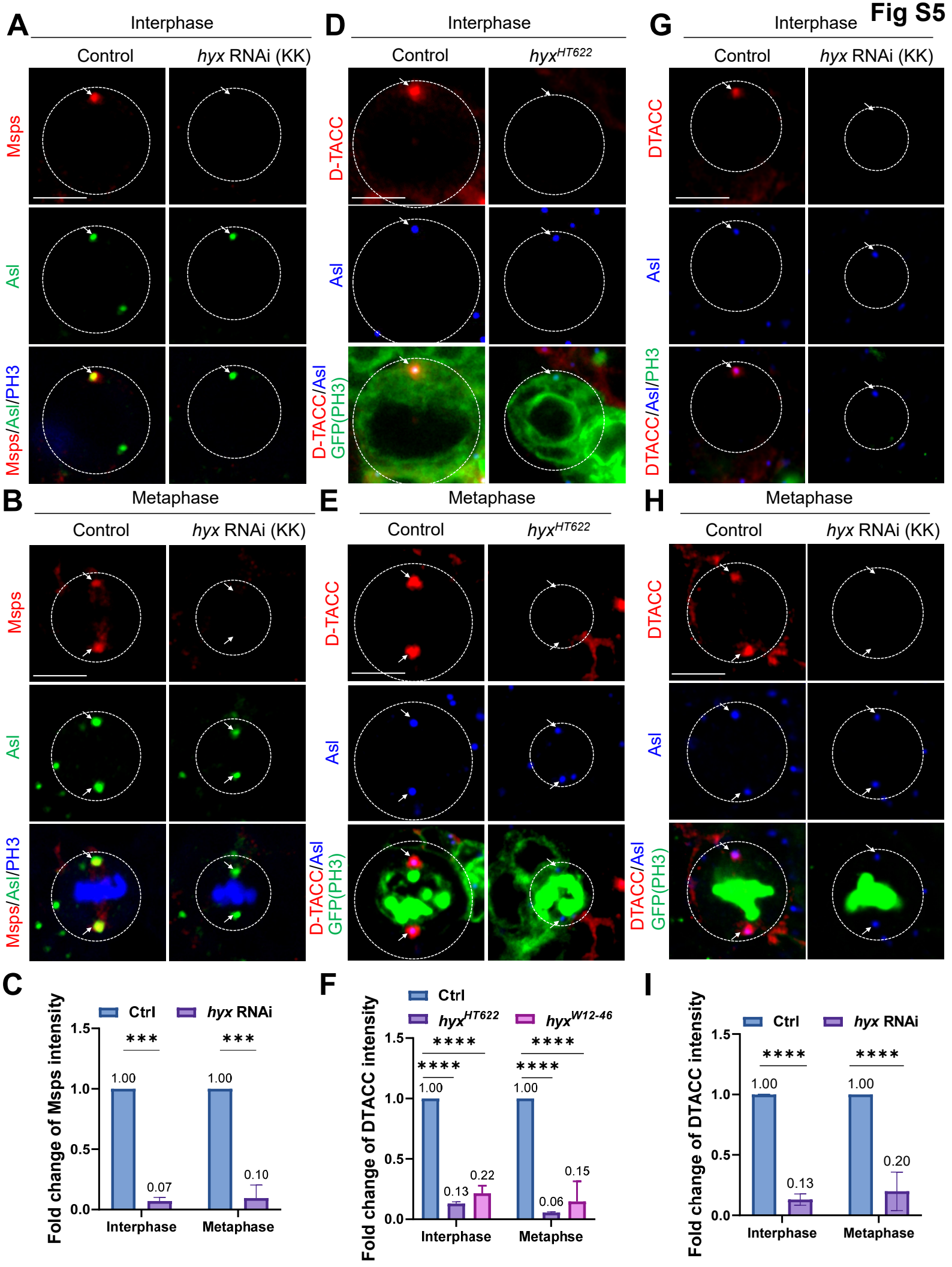
Fig S5
A
Interphase
Control
hyx RNAi (KK)
Msps
Asl
Msps/Asl/PH3
D
Interphase
Control
hyxHT622
D-TACC
Asl
D-TACC/Asl
GFP(PH3)
G
Interphase
Control
hyx RNAi (KK)
DTACC
Asl
DTACC/Asl/PH3
B
Metaphase
Control
hyx RNAi (KK)
Msps
Asl
Msps/Asl/PH3
E
Metaphase
Control
hyxHT622
D-TACC
Asl
D-TACC/Asl
GFP(PH3)
H
Metaphase
Control
hyx RNAi (KK)
DTACC
Asl
DTACC/Asl
GFP(PH3)
C
Fold change of Msps intensity
Ctrl
hyx RNAi
***
***
1.00
0.07
1.00
0.10
Interphase
Metaphase
F
Fold change of DTACC intensity
Ctrl
hyxHT622
hyxW12-46
****
****
****
****
1.00
0.13
0.22
1.00
0.06
0.15
Interphase
Metaphse
I
Fold change of DTACC intensity
Ctrl
hyx RNAi
****
****
1.00
0.13
1.00
0.20
Interphase
Metaphase

Fig S6

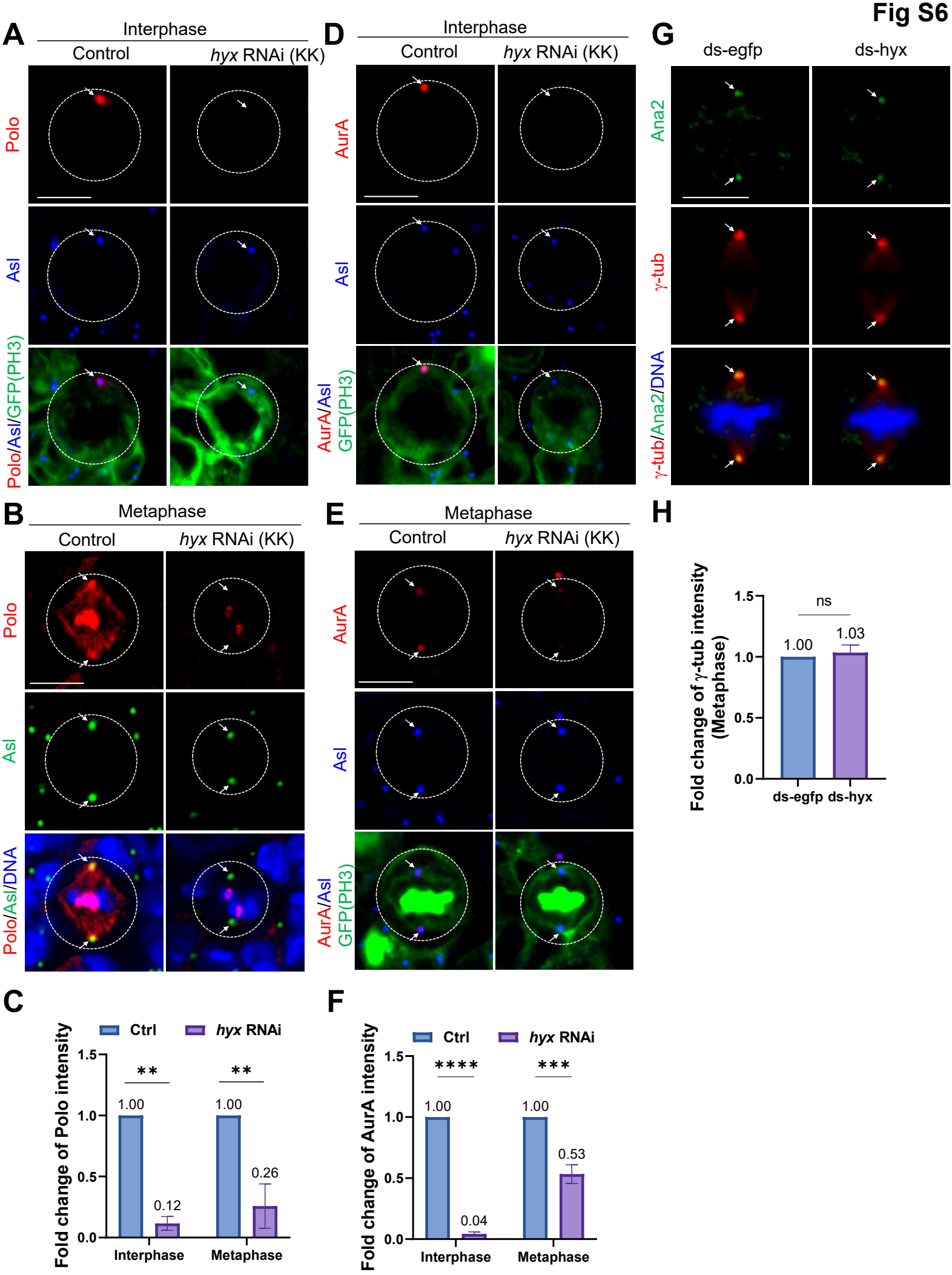
A
Interphase
Control
hyx RNAi (KK)
Polo
Asl
Polo/Asl/GFP(PH3)
B
Metaphase
Control
hyx RNAi (KK)
Polo
Asl
Polo/Asl/DNA
C
Ctrl
hyx RNAi
Fold change of Polo intensity
1.5
1.0
0.5
0.0
**
**
1.00
0.12
1.00
0.26
Interphase
Metaphase
D
Interphase
Control
hyx RNAi (KK)
AurA
Asl
AurA/Asl
GFP(PH3)
E
Metaphase
Control
hyx RNAi (KK)
AurA
Asl
AurA/Asl
GFP(PH3)
F
Ctrl
hyx RNAi
Fold change of AurA intensity
1.5
1.0
0.5
0.0
****
***
1.00
0.04
1.00
0.53
Interphase
Metaphase
G
ds-egfp
ds-hyx
Ana2
γ-tub
γ-tub/Ana2/DNA
H
Fold change of γ-tub intensity
(Metaphase)
1.5
1.0
0.5
0.0
ns
1.00
1.03
ds-egfp
ds-hyx